ARTICLE

https://doi.org/10.1038/s41586-019-1325-x

TOX transcriptionally and epigenetically programs CD8$^+$ T cell exhaustion

Omar Khan[1,2,3,14], Josephine R. Giles[1,2,3], Sierra McDonald[4,5,6], Sasikanth Manne[1,2], Shin Foong Ngiow[1,2,3], Kunal P. Patel[1,2,7], Michael T. Werner[4,6], Alexander C. Huang[2,3,7], Katherine A. Alexander[4,5,6], Jennifer E. Wu[1,2,3], John Attanasio[1,2], Patrick Yan[1,2], Sangeeth M. George[1,2], Bertram Bengsch[8,9], Ryan P. Staupe[1,2], Greg Donahue[4,5,6], Wei Xu[10], Ravi K. Amaravadi[7,10], Xiaowei Xu[10,11], Giorgos C. Karakousis[10,12], Tara C. Mitchell[7,10], Lynn M. Schuchter[7,10], Jonathan Kaye[13], Shelley L. Berger[4,5,6] & E. John Wherry[1,2,3]*

Exhausted CD8$^+$ T (T_{ex}) cells in chronic infections and cancer have limited effector function, high co-expression of inhibitory receptors and extensive transcriptional changes compared with effector (T_{eff}) or memory (T_{mem}) CD8$^+$ T cells. T_{ex} cells are important clinical targets of checkpoint blockade and other immunotherapies. Epigenetically, T_{ex} cells are a distinct immune subset, with a unique chromatin landscape compared with T_{eff} and T_{mem} cells. However, the mechanisms that govern the transcriptional and epigenetic development of T_{ex} cells remain unknown. Here we identify the HMG-box transcription factor TOX as a central regulator of T_{ex} cells in mice. TOX is largely dispensable for the formation of T_{eff} and T_{mem} cells, but it is critical for exhaustion: in the absence of TOX, T_{ex} cells do not form. TOX is induced by calcineurin and NFAT2, and operates in a feed-forward loop in which it becomes calcineurin-independent and sustained in T_{ex} cells. Robust expression of TOX therefore results in commitment to T_{ex} cells by translating persistent stimulation into a distinct T_{ex} cell transcriptional and epigenetic developmental program.

After activation by an antigen, naive CD8$^+$ T cells undergo extensive molecular rewiring into T_{eff} cells[1]. If the antigen is cleared, a subset of T_{eff} cells persist and form long-lived, self-renewing T_{mem} cells that are capable of mounting rapid recall responses[1]. By contrast, during chronic infections or cancer, this differentiation is diverted and T cells can instead become exhausted[2]. T_{ex} cells may balance partial pathogen or tumour control while restraining immunopathology. The consequence of restrained functionality, however, is disease persistence and/or progression[3,4]. T cell exhaustion is a common feature of many chronic infections and cancers in mice and humans[5–8]; indeed, T_{ex} cells are a major target of checkpoint blockade in patients with cancer[3,9–11].

T_{ex} cells are characterized by the hierarchical loss of cytokine production (IL-2, TNF, IFNγ), high co-expression of inhibitory receptors (such as PD-1, LAG-3, TIGIT), altered metabolism, and impaired proliferative potential and survival[2]. T_{ex} cells also display a distinct transcriptional program that is highlighted by the altered use of key transcription factors[12]. Moreover, recent epigenetic analysis revealed that T_{ex} cells differ from T_{eff} and T_{mem} cells by approximately 6,000 open chromatin regions[13–16], which is similar to the differences between other major haematopoietic lineages[17]. T_{ex} cells are therefore not simply a state of activation of T_{eff} or T_{mem} cells, but rather they are a distinct cell type. However, the mechanisms that initiate the fate commitment and epigenetic and transcriptional programming of T_{ex} cells remain unknown.

Here we identify a requisite role for the HMG-box transcription factor TOX in programming the early epigenetic events that drive the fate commitment of T_{ex} cells. Although it is robustly expressed in T_{ex} cells, TOX is only transiently expressed at low levels during acute infections. Moreover, T_{eff} and T_{mem} cells can form without TOX, whereas T_{ex} cells cannot. TOX is necessary and sufficient to induce major features of T_{ex} cells, including the expression of inhibitory receptors, decreased function and the expression of transcription factors that are required for T_{ex} cells. TOX translates early, sustained NFAT2 activity into a subsequent calcineurin-independent TOX-driven molecular and epigenetic T_{ex} program. Furthermore, TOX represses terminal T_{eff}-cell-specific epigenetic events while initiating key T_{ex}-cell-specific epigenetic changes. These data identify TOX as a critical transcriptional and epigenetic coordinator of T_{ex} cell programming. Moreover, these observations have implications for the ontogeny of T_{ex} cells and therapeutic opportunities.

Tox is selectively upregulated in developing T_{ex} cells

We first analysed transcription data from virus-specific mouse CD8$^+$ T cells responding to acute (Armstrong) or chronic (clone 13) lymphocytic choriomeningitis mammarenavirus (LCMV) infection. By day 6 post-infection, we detected considerable divergence of gene expression (Fig. 1a). We proposed that genes that have chromatin-modulating capacity could drive distinct transcriptional trajectories in developing T_{mem} and T_{ex} cells. Indeed, gene ontology analysis identified differentially expressed gene families with chromatin-binding and transcription-factor activity (Fig. 1b). Moreover, genes within these families were differentially engaged during T cell differentiation, suggesting distinct chromatin modulators that were involved in T_{eff}, T_{mem} and T_{ex} cell

[1]Department of Systems Pharmacology and Translational Therapeutics, Perelman School of Medicine, University of Pennsylvania, Philadelphia, PA, USA. [2]Institute for Immunology, Perelman School of Medicine, University of Pennsylvania, Philadelphia, PA, USA. [3]Parker Institute for Cancer Immunotherapy, Perelman School of Medicine, University of Pennsylvania, Philadelphia, PA, USA. [4]Epigenetics Institute, Perelman School of Medicine, University of Pennsylvania, Philadelphia, PA, USA. [5]Department of Cell and Developmental Biology, Perelman School of Medicine, University of Pennsylvania, Philadelphia, PA, USA. [6]Department of Genetics, Perelman School of Medicine, University of Pennsylvania, Philadelphia, PA, USA. [7]Department of Medicine, Perelman School of Medicine, University of Pennsylvania, Philadelphia, PA, USA. [8]Department of Medicine II: Gastroenterology, Hepatology, Endocrinology, and Infectious Disease, University Medical Center Freiburg, Freiburg, Germany. [9]BIOSS Centre for Biological Signaling Studies, Freiburg, Germany. [10]Abramson Cancer Center, Perelman School of Medicine, University of Pennsylvania, Philadelphia, PA, USA. [11]Department of Pathology and Laboratory Medicine, Perelman School of Medicine, University of Pennsylvania, Philadelphia, PA, USA. [12]Department of Surgery, Perelman School of Medicine, University of Pennsylvania, Philadelphia, PA, USA. [13]Research Division of Immunology, Department of Biomedical Sciences, Cedars-Sinai Medical Center, Los Angeles, CA, USA. [14]Present address: Arsenal Biosciences, South San Francisco, CA, USA. *e-mail: wherry@pennmedicine.upenn.edu

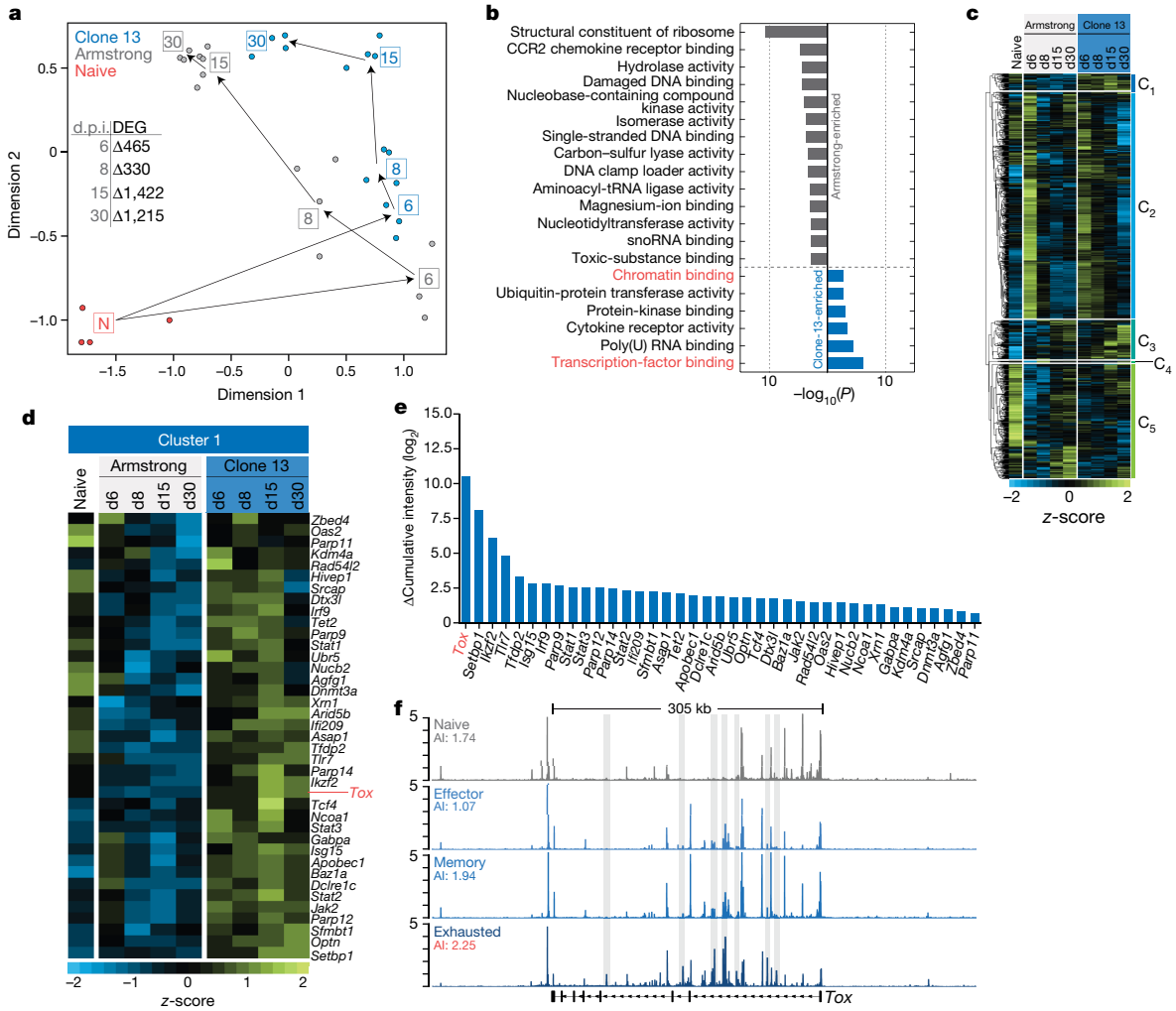

Fig. 1 | Multiple epigenetic modulators, including TOX, are selectively expressed in T_{ex} cells. a, Multidimensional scaling analysis of transcriptional data from naive LCMV-specific $CD8^+$ T cells from P14 mice or from T cells after acute (Armstrong) or chronic (clone 13) LCMV infection at the indicated days post-infection (d.p.i.). The table (inset) enumerates differentially expressed genes (DEG; false discovery rate (FDR) < 0.05) between T cells during infection with Armstrong and clone 13 at the specified days post-infection. **b**, Gene ontology analysis of differentially expressed genes 6 days post-infection with Armstrong or clone 13. Grey and blue colours denote gene ontology molecular functions enriched in Armstrong and clone 13, respectively. Categories that include chromatin-binding proteins are highlighted in red. **c**, Heat map of differentially expressed chromatin-modulating genes (Supplementary Table 8, see Methods) between naive P14 T cells and P14 T cells during infection with Armstrong or clone 13. d, day. Genes are ordered by hierarchical clustering using Manhattan distance and clusters generated by *k*-means. Shown are the *z*-scores of $\log_2$ expression data. **d**, Chromatin modulating genes in cluster 1. **e**, Difference in cumulative expression of genes in cluster 1. The values were calculated by summing the normalized array intensity of each gene at all time points post-infection and subtracting values from Armstrong infection from those of clone-13 infection. **f**, ATAC–seq tracks of in vivo naive T, T_{eff}, T_{mem} and T_{ex} cells from P14 mice at the *Tox* locus. The accessibility index (AI) of each sample is calculated by summing the normalized tag counts across the locus and dividing by its length.

differentiation (Fig. 1c, Extended Data Fig. 1a, Supplementary Table 1). Genes in cluster 1 were biased to chronic infection and included those that encode several transcription factors (*Stat1*, *Stat2*, *Tcf4*, *Ikzf2*) and chromatin modulators (*Tet2*, *Dnmt3a*) with roles in T cell exhaustion[18,19], as well as genes with uncharacterized functions in T_{ex} cells, including *Setbp1*, *Kdm4a* and *Tox* (Fig. 1d, Extended Data Fig. 1a, b). Among these, *Tox* was the most differentially expressed in developing T_{ex} cells when compared with T_{eff} and T_{mem} cells (Fig. 1e).

TOX is involved in the development of natural killer, innate lymphoid-like, and $CD4^+$ T cells[20,21]. However, the role of TOX in peripheral $CD8^+$ T cells is poorly understood. Previous network analyses found TOX to be the most differentially connected transcription factor between T_{mem} and T_{ex} cells, which suggests that it has a prominent role in T_{ex} cells[12]. Moreover, chromatin accessibility of the *Tox* locus was increased in T_{ex} compared to T_{eff} cells, suggesting epigenetic remodelling of *Tox* in T_{ex} cells (Fig. 1f). The *Tox* locus contained a dense cluster of open chromatin regions, a feature associated with 'stretch' or 'super' enhancers[22,23]. Such 'super' enhancers often demarcate genes or loci that are involved in cell fate decisions[23]. Among loci with large stretches of open chromatin, *Tox* ranked much more highly in T_{ex} cells (rank = 35) compared to naive T, T_{eff} and T_{mem} cells (rank = 91, 365 and 64, respectively) (Extended Data Fig. 1c). Together, these data lead to the hypothesis that TOX may act as a central node in the differentiation of T_{ex} cells.

High and sustained TOX is associated with exhaustion

The expression of TOX significantly increased by day 4 of clone-13 infection, and approximately 80% of LCMV-specific P14 $CD8^+$ T cells expressed high TOX by day 5 post-infection (Fig. 2a). Moreover, high TOX expression was sustained in more than 95% of T_{ex} cells from day 15 post-infection onwards, and it remained highly expressed for more than 200 days after infection (Fig. 2a, Extended Data Fig. 2a). By contrast, although TOX was initially expressed in some T_{eff} cells that responded to Armstrong infection, its expression peaked

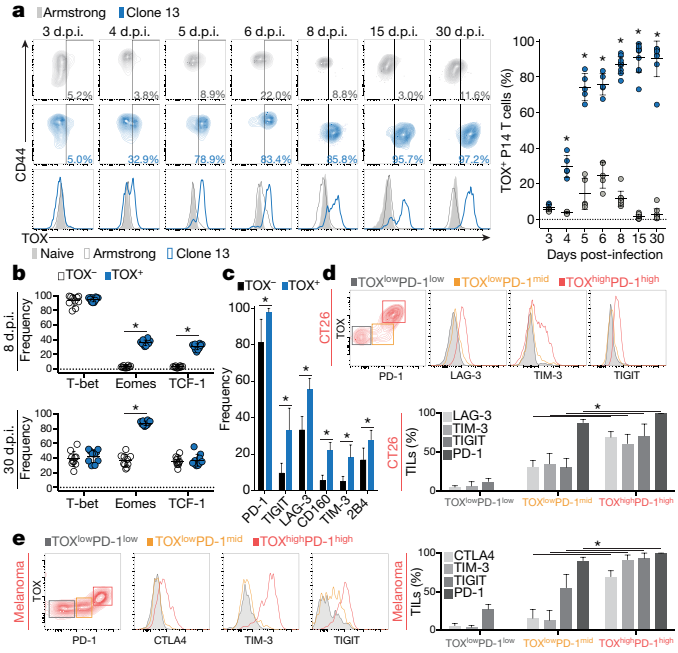

Fig. 2 | Rapid and sustained TOX expression is associated with key features of exhaustion. a, TOX protein expression in P14 T cells after infection with Armstrong or clone 13 at the indicated days post-infection. Frequencies of TOX^+ P14 T cells relative to total P14 T cell population (left) and summary data (right). **b**, Transcription-factor expression within TOX^+ and TOX^- P14 T cell populations at day 8 or day 30 after clone-13 infection. **c**, Inhibitory-receptor expression in TOX^+ and TOX^- P14 T cells at day 30 after clone-13 infection. **d**, **e**, Identification of TOX-expressing cells in TILs from CT26 carcinoma mouse model (**d**) and human melanoma biopsy samples (**e**). TOX and inhibitory-receptor expression in $TOX^{low}PD\text{-}1^{low}$, $TOX^{low}PD\text{-}1^{mid}$ and $TOX^{high}PD\text{-}1^{high}$ TIL populations. Contour and histogram plots are representative of at least three independent experiments consisting of at least four mice. Unless otherwise noted, P14 T cells were analysed from the spleens of infected mice. Summarized experiments denote one mouse per data point and error is reported as s.d. For **e**, 5 human TIL and 11 human normal donor samples were analysed. Statistical significance ($*P < 0.01$) was determined using the Student's *t*-test.

at 5–6 days post-infection and was limited to less than 25% of the population. Moreover, the amount of TOX per cell was low and expression was transient, returning to near-baseline levels between day 8–15 post-infection (Fig. 2a). Thus, high and sustained levels of TOX were observed only during chronic infection. Notably, the difference in TOX expression emerged before the time at which the virological outcomes diverged (around 8 days post-infection)[24], which suggests that viral load alone was not a primary driver of differential expression.

Whereas $CD127^+KLRG1^-$ cells contained both TOX^+ and TOX^- cells early in clone-13 infection, TOX^- cells were enriched in the $CD127^-KLRG1^+$ subset, which suggests a negative relationship between TOX and $KLRG1^+$ terminal effector cells[25–27] (Extended Data Fig. 2b). This $KLRG1^+$ terminal effector population is unable to generate T_{ex} cells, perhaps owing to a lack of TCF-1 and Eomes[27–29]. Indeed, TCF-1 and Eomes expression was confined mainly to the TOX^+ cells at day 8 post-infection (Fig. 2b, Extended Data Fig. 2c, top). Although both TCF-1 subsets expressed TOX later in clone-13 infection, higher TOX correlated with higher Eomes[28] (Fig. 2b, Extended Data Fig. 2c, bottom). TOX^+ cells also had high expression of PD-1, TIGIT, LAG-3 and CD160 throughout clone-13 infection (Fig. 2c, Extended Data Fig. 2d, e). Therefore, TOX expression was negatively correlated with the development of $KLRG1^+$ terminal T_{eff} cells, and instead was associated with high expression of inhibitory receptors and key T_{ex} cell transcription factors.

TOX expression in the setting of other acute infections was limited to the peak of the effector phase and rapidly decreased over time (Extended Data Fig. 2f). By contrast, the majority of tumour-infiltrating $CD8^+$ T lymphocytes (TILs) in B16F10 (B16) or CT26 tumours had high levels of TOX, and a high frequency of human melanoma TILs also expressed TOX (Extended Data Fig. 2g). Additionally, the analysis of single-cell RNA expression data from TILs of patients with non-small-cell lung cancer or hepatocellular carcinoma showed that *TOX* expression was limited to the T_{ex} cell subset (Extended Data Fig. 2h). In TILs from mice and humans, there was a strong association between high TOX and high co-expression of inhibitory receptors (Fig. 2d, e, Extended Data Fig. 2g). Finally, TOX expression in tumour-specific TILs was negatively associated with the production of inflammatory cytokines, which suggests that TOX may regulate T cell function in tumours (Extended Data Fig. 2i).

An essential role for TOX in the generation of T_{ex} cells

To further investigate the role of TOX in T_{ex} cells, we generated $Tox^{flox/flox}Cd4^{cre}$ P14 mice (hereafter denoted TOX cKO). Naive T cells from TOX cKO P14 mice were mixed in a 1:1 ratio with T cells from wild-type P14 mice and adoptively transferred into new mice (Extended Data Fig. 3a, b). In chronic infection, TOX cKO P14 T cells mounted an initial response, but then rapidly declined in number and were not sustained past day 15 post-infection, unlike wild-type P14 T cells that persisted (Fig. 3a, Extended Data Fig. 3c). This decline was not due to rejection, because escaped TOX^+ cells could readily be detected long-term and both TOX cKO and wild-type P14 T cells initially proliferated similarly based on the analysis of Ki-67 (Extended Data Fig. 3d, e). Moreover, TOX cKO cells that responded to acutely resolved LCMV Armstrong generated robust T_{eff} and T_{mem} cells that were detectable for more than 30 days (Fig. 3a). Thus, TOX cKO $CD8^+$ T cells were not intrinsically unable to form $CD8^+$ T cells that could persist after acute infection, including T_{mem} cells, but rather they had a specific defect in the ability to generate T_{ex} cells.

TOX cKO P14 T cells generated more $KLRG1^+CD127^-$ T_{eff} cells in both acute and chronic infection (Fig. 3b, Extended Data Fig. 3f). However, in Armstrong infection, TOX cKO cells effectively generated typical T_{mem} cell populations (Extended Data Fig. 3g–k). In chronic infection, TOX cKO cells expressed lower levels of PD-1, CD160, LAG-3 and TIGIT (Fig. 3c). By contrast, levels of 2B4 and TIM-3 were increased in the absence of TOX, in agreement with previous studies that showed a negative correlation between PD-1 and TIM-3 early in clone-13 infection[30] (Fig. 3c). TOX deficiency also improved function (Fig. 3d). Because complete TOX deficiency resulted in an inability to sustain T_{ex} cell responses, we next asked whether the conditional deletion of one allele would enhance tumour immunity. Indeed, partially TOX-deficient tumour-specific T cells controlled tumour growth significantly better than wild-type cells (Fig. 3e).

The establishment and maintenance of T_{ex} cells depends on a proliferative hierarchy mediated by TCF-1, T-bet and Eomes[28–30]. We therefore examined the expression of these transcription factors in the absence of TOX in T_{ex} cells. The expression of Eomes was reduced in the absence of TOX, whereas that of T-bet was unaffected (Fig. 3f). TCF-1 expression was nearly ablated in TOX cKO $CD8^+$ T cells during chronic infection with a near absence of the $TCF\text{-}1^+$ subset of T_{ex} cells (Fig. 3f). Notably, there was no defect in TCF-1 expression by naive TOX cKO cells, and TOX cKO T_{mem} cells that were generated after acute infection retained the ability to express TCF-1 and Eomes (Extended Data Fig. 3b, h). These data suggest that a primary defect in TOX cKO T_{ex} cells is the inability to rewire the transcriptional control of TCF-1 and/or Eomes after initial development of T_{ex} cell precursors, with a resulting loss of the $TCF\text{-}1^+$ subset of T_{ex} cells.

Transcriptional analysis of wild-type and $Tox^{-/-}$ P14 T cells on day 8 of clone-13 infection revealed the differential expression of more than 3,100 genes. A major feature of these data was the upregulation in TOX-deficient P14 T cells of many genes associated with T_{eff} cells—including *Klrg1*, *Gzma*, *Gzmb*, *Cx3cr1*, *Zeb2* and *Prf1* (Fig. 3g, Supplementary Table 2). By contrast, downregulated genes included *Pdcd1* and *Cd160*,

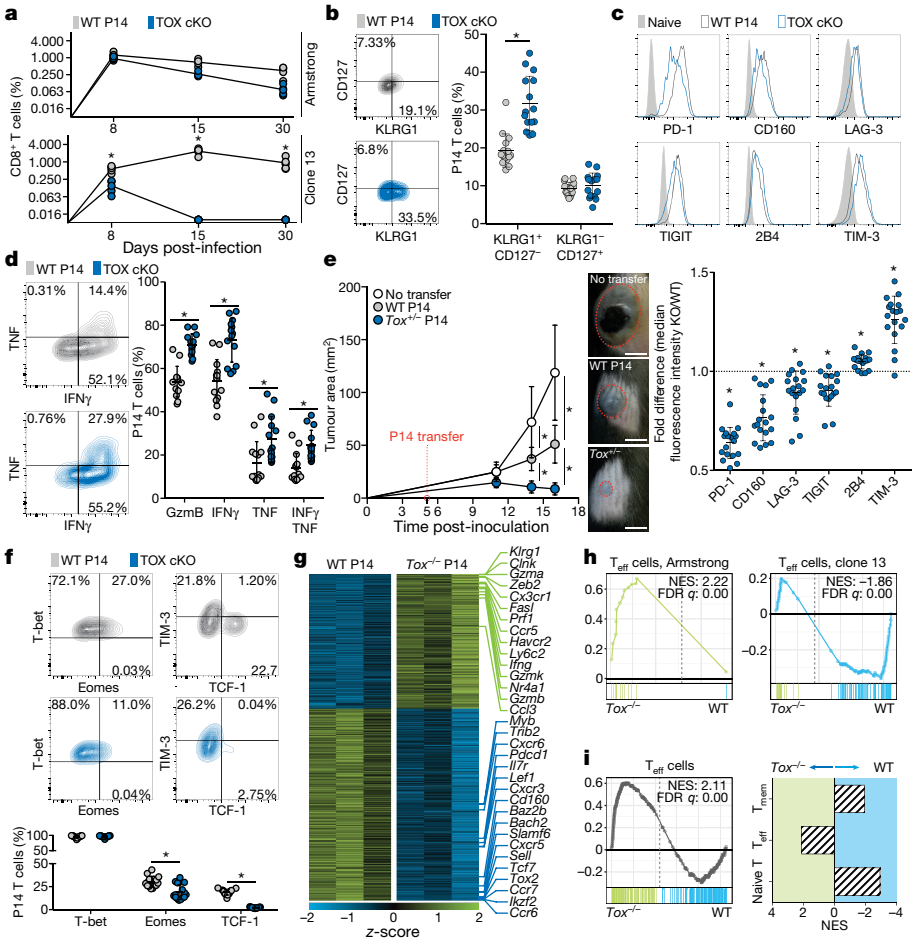

Fig. 3 | TOX is required for the development of T_{ex} cells. Wild-type (WT) and TOX cKO T cells from P14 mice were mixed in a 1:1 ratio and adoptively transferred into host mice. Spleens were collected at the indicated time points after infection with Armstrong or clone 13 (**a**) or on day 8 of clone-13 infection (**b**–**d**, **f**). **a**, Frequency of wild-type or TOX cKO T cells relative to the total $CD8^+$ T cell pool during infection with Armstrong (top) or clone 13 (bottom). **b**–**d**, KLRG1 and CD127 (**b**), inhibitory receptor (**c**) and cytokine (**d**) expression in wild-type and TOX cKO P14 T cells. Summary of changes in the expression of inhibitory receptors displayed as the ratio of the median fluorescence intensity of inhibitory receptors between TOX cKO and wild-type P14 T cells. **e**, Tumour area after inoculation with B16-GP33 and transfer of pre-activated wild-type or $Tox^{+/-}$ P14 T cells. Scale bars, 5 mm. **f**, Expression of transcription factors in wild-type and TOX cKO P14 T cells. **g**–**i**, Wild-type and $Tox^{-/-}$ P14 T cells were mixed in a 1:1 ratio, transferred into wild-type hosts, and recovered from the spleen on day 8 of clone-13 infection for RNA sequencing. **g**, Differentially expressed genes in wild-type compared with $Tox^{-/-}$ P14 T cells. Genes associated with T_{eff} or T_{mem} cells are labelled. Each column represents a biological replicate. **h**, Gene set enrichment analysis (GSEA) of the transcriptional signature from early (day 8) T cell responses to acute (T_{eff} cells, Armstrong, left) or chronic (T_{eff} cells, clone-13, right) infection in $Tox^{-/-}$ versus wild-type P14 T cells[12]. NES, normalized enrichment score. **i**, GSEA and normalized enrichment scores of transcriptional signatures associated with naive T, T_{eff} or T_{mem} cells compared to the differentially expressed genes in $Tox^{-/-}$ versus wild-type P14 T cells. Contour and histogram plots are representative of at least four independent experiments consisting of at least four mice. Heat maps were generated using *z*-scores derived from $\log_2$ tag counts. Statistical significance ($^*P < 0.01$) was determined using the Student's *t*-test, error is reported as s.d.

as well as a number of genes associated with T cell or T_{ex} cell progenitor biology including *Myb*, *Il7r*, *Cxcr5*, *Slamf6*, *Lef1* and *Tcf7* (Fig. 3g). Indeed, in clone-13 infection in the absence of TOX, there was strong enrichment of the signature from T_{eff} cells generated during LCMV Armstrong infection, whereas the signature of T_{ex} cell precursors was depleted (Fig. 3h). These data suggest that TOX is necessary to program early transcriptional responses to clone-13 infection. Moreover, the increased signature of short-lived $KLRG1^+$ effectors that are incapable of giving rise to T_{ex} cells could relate to increased TCR signalling due to reduced expression of inhibitory receptors in the absence of TOX[25,26] (Fig. 3i, Extended Data Fig. 3l, m). Finally, enrichment of the T_{eff} cell signature in $Tox^{-/-}$ cells was not due solely to the loss of *Tcf7* expression, as only a minor proportion of the total transcriptional signature can be accounted for by the signature of $Tcf7^{-/-}$ T cells[30] (Extended Data Fig. 3n). Collectively, these findings suggest that TOX promotes the generation of T_{ex} cells by fostering key developmental hallmarks of exhaustion while repressing development of the $KLRG1^+$ T_{eff} cell lineage.

Induction of TOX requires calcium signalling and NFAT2

In $CD4^+CD8^+$ thymocytes, TOX expression depends on calcineurin signalling[31]. Indeed, the calcium ionophore ionomycin—which induces calcium flux and calcineurin signalling—induced TOX expression in naive $CD8^+$ T cells, whereas treatment with the protein kinase C activator phorbol myristate acetate alone or in combination with ionomycin failed to induce TOX (Fig. 4a). These results suggested that TOX expression in mature $CD8^+$ T cells was primarily regulated by calcineurin-mediated signalling. Calcineurin signalling operates primarily through NFAT proteins[32], and analysis of NFAT1[33] and NFAT2[34] DNA-binding data from T_{eff} cells indicated that both were capable of binding to the *Tox* locus (Fig. 4b). We focused here on NFAT2, because the gene that encodes this protein (*Nfatc1*) is differentially expressed in T_{ex} compared with T_{eff} and T_{mem} cells (Extended Data Fig. 4a). Retroviral expression of a constitutively active and nucleus-restricted mutant (CA-NFAT2) induced TOX in vitro, whereas wild-type NFAT2 did not[35] (Fig. 4c, Extended Data Fig. 4b). Moreover, NFAT2 cKO P14 T cells (from $Nfatc1^{flox/flox}Cd4^{cre}$ P14 mice) failed to express TOX in vivo

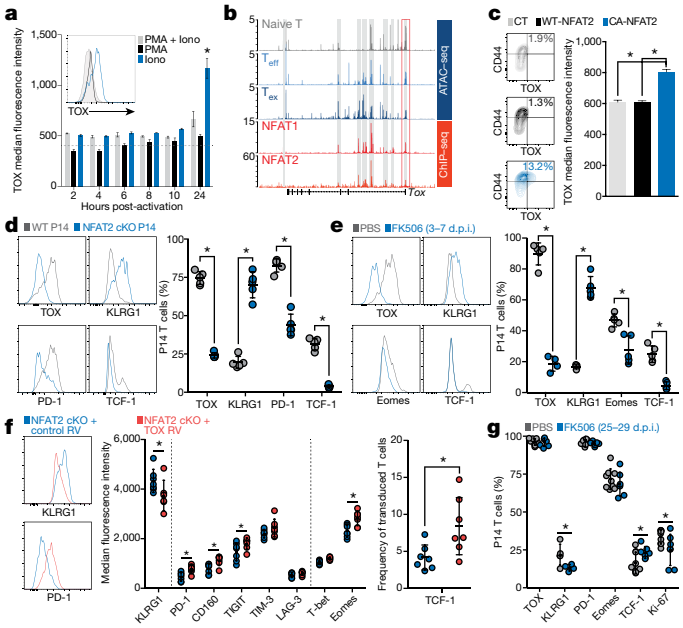

Fig. 4 | Calcineurin signalling and NFAT2 are necessary and sufficient to induce TOX, but sustained expression becomes calcineurin-independent. a, Inset, TOX expression in $CD8^+$ T cells after 24 h of stimulation with phorbol myristate acetate (PMA), ionomycin (Iono) or phorbol myristate acetate in combination with ionomycin. The main graph shows the time course of the median fluorescence intensity of TOX after addition of the stimulus; the dashed line indicates the median fluorescence intensity of TOX in naive T cells. **b**, ATAC–seq tracks of the *Tox* locus in naive T, T_{eff} and T_{ex} P14 T cells compared with NFAT1 (red) and NFAT2 (orange) chromatin immunoprecipitation with sequencing (ChIP–seq) tracks from T_{eff} cells[33,34]. The promoter region is highlighted with a red box. Grey bars highlight significant enrichment of NFAT1 and NFAT2. **c**, TOX expression in wild-type-NFAT2, CA-NFAT2, or mock-transduced T cells. **d**, Wild-type and *Nfatc1*$^{flox/flox}$*Cd4*^{cre} P14 T cells were mixed in a 1:1 ratio and adoptively transferred into wild-type hosts before infection with clone 13. The graphs show the frequency of TOX^+, $KLRG1^+$, $PD\text{-}1^+$ and $TCF\text{-}1^+$ P14 T cells on day 8 post-infection. **e**, TOX, KLRG1, PD-1 and TCF-1 expression in P14 T cells on day 8 post-infection with clone 13, after treatment with FK506 or PBS from day 3–7. **f**, NFAT2 cKO P14 T cells were transduced with a retrovirus (RV) encoding TOX (NFAT2 cKO + TOX) or control GFP (NFAT2 cKO + control) and adoptively transferred into wild-type congenic mice infected with clone 13. T_{eff} markers, inhibitory receptors and transcription factors were evaluated on day 7 post-infection. **g**, Expression of T_{eff} markers, inhibitory receptors and transcription factors measured on day 30 post-infection with clone 13 after treatment with FK506 or PBS on day 25–29. Contour and histogram plots are representative of at least three independent experiments consisting of at least three mice per group. Unless otherwise noted, P14 T cells were analysed from the spleens of infected mice. Statistical significance ($^*P < 0.01$) was determined using the Student's *t*-test, error is reported as s.d.

during clone-13 infection (Fig. 4d, Extended Data Fig. 4c). NFAT2-deficient P14 T cells phenocopied TOX cKO P14 T cells and failed to generate T_{ex} cell precursors, instead producing T_{eff} cells with increased expression of KLRG1 and lower PD-1 and TCF-1 (Fig. 4d). To complement the NFAT2 cKO approach, clone-13-infected mice containing wild-type P14 T cells were treated with the calcineurin inhibitor FK506 starting at day 3 post-infection. Treatment between day 3 and day 7 post-infection had a minimal effect on overall T cell activation, as measured by CD44 expression, but significantly reduced TOX expression (Fig. 4e, Extended Data Fig. 4d). Moreover, P14 T cells from mice that were treated with FK506 phenocopied TOX-deficient T cells, based on the high expression of KLRG1, low expression of Eomes, and a lack of TCF-1 (Fig. 4e). Retroviral expression of TOX in NFAT2-deficient T cells restored the expression of PD-1 and other inhibitory receptors, while increasing the expression of Eomes and TCF-1 and significantly reducing that of KLRG1 (Fig. 4f, Extended Data Fig. 4e). Thus, calcineurin and NFAT2 are required to induce TOX. However, enforced TOX expression in NFAT2-cKO cells can restore early T_{ex} differentiation, which demonstrates a key role for TOX as an inducer of T_{ex} differentiation downstream of NFAT2.

We next tested whether continuous calcium and NFAT signalling were required for the sustained TOX expression once exhaustion was established. Treatment with FK506 or cyclosporin A between day 25 and day 29 of chronic infection reduced the expression of Ki-67 in T_{ex} cells (Fig. 4g, Extended Data Fig. 4f, g), as expected owing to the requirement of TCR signalling to drive the proliferative hierarchy of T_{ex} cells[28]. Although the treatment of established T_{ex} cells in vivo slightly enriched the progenitor T_{ex} cell subset ($TCF\text{-}1^{high}$), there was little effect on TOX expression and essentially all virus-specific T_{ex} cells remained TOX^+ (Fig. 4g, Extended Data Fig. 4g). Moreover, the expression of PD-1 and Eomes remained essentially unchanged (Fig. 4g, Extended Data Fig. 4g). These data indicate that although initial TOX induction requires NFAT2, TOX expression and the TOX-dependent T_{ex} cell program become independent of calcineurin signalling once established.

A program of exhaustion induced by TOX

We next tested whether TOX was sufficient to drive exhaustion. Retroviral TOX expression in vitro reduced cytokine production while increasing PD-1 (Fig. 5a, b). To test whether these TOX-induced changes were durable in vivo, P14 T cells were transduced with *Tox* retrovirus and transferred into LCMV Armstrong-infected mice. In vivo, TOX expression reduced the frequency of $KLRG1^+$ T_{eff} cells, increased inhibitory-receptor expression, and reduced function (Extended Data Fig. 5a–c). Moreover, retrovirally expressed TOX reduced the expression of T-bet and increased that of TCF-1 (Extended Data Fig. 5d). Thus, enforced TOX expression drove key features of T_{ex} cells, skewed differentiation away from T_{eff} and T_{mem} cells, and sustained these effects for more than 30 days (Extended Data Fig. 5e, f). RNA sequencing of retrovirally transduced $CD8^+$ T cells in vitro revealed a downregulation of T_{mem} cell signatures and an upregulation of genes involved in exhaustion[12,36] (Fig. 5c, Extended Data Fig. 5g, Supplementary Table 3). Indeed, many key individual exhaustion genes—such as those encoding inhibitory receptors (*Pdcd1*, *Lag3*, *Ctla4*) and transcription factors (*Nr4a2*, *Ikzf3*, *Tox2*, *Bhlhe41*)—were induced by retrovirus-mediated TOX expression in vitro, whereas memory-associated genes (*Ccr7*, *Il7r* and *Sell*) were repressed (Fig. 5d). Moreover, even in an unrelated cell type (NIH3T3 fibroblasts) TOX was found to induce expression of multiple immune pathways—including those associated with inflammatory cytokine production, T cell activation and proliferation as well as calcineurin and NFAT signalling (Fig. 5e, Extended Data Fig. 5h, i). Additionally, the transcriptional signature induced by TOX in fibroblasts was enriched in the signature of in vivo T_{ex} cells (Fig. 5f, Extended Data Fig. 5j, Supplementary Table 4). Thus, TOX was capable of inducing a transcriptional program of T_{ex} cells, and could even do so—at least partially—in an unrelated cell type. This is reminiscent of the related HMG transcription factor TCF-1, which can induce the expression of naive T cell genes in fibroblasts[37].

Epigenetic programming of T_{ex} cells by TOX

It has recently been demonstrated that T_{ex} cells have a unique epigenetic landscape compared to naive T, T_{eff} and T_{mem} cells[13–16]. Thus, we next asked whether TOX regulated this epigenetic commitment of T_{ex} cells. In the absence of TOX there were around 4,000 regions for which chromatin accessibility was altered—as measured by an assay for transposase-accessible chromatin with high-throughput sequencing (ATAC–seq)—on day 8 of clone-13 infection. Over 70% of these changes were in intronic or intergenic regions that were consistent with enhancers, whereas 20% were at promoters or transcription start sites (Extended Data Fig. 6a, Supplementary Table 5). Among these changes were increases in chromatin accessibility at genes associated with terminal T_{eff} cell differentiation—including *Klrg1*, *Gzma*, *Gzmb*, *Gzmm*, *Clnk*, *Zeb2* and *Nr4a1* (Fig. 6a, b, Extended Data Fig. 6b)—

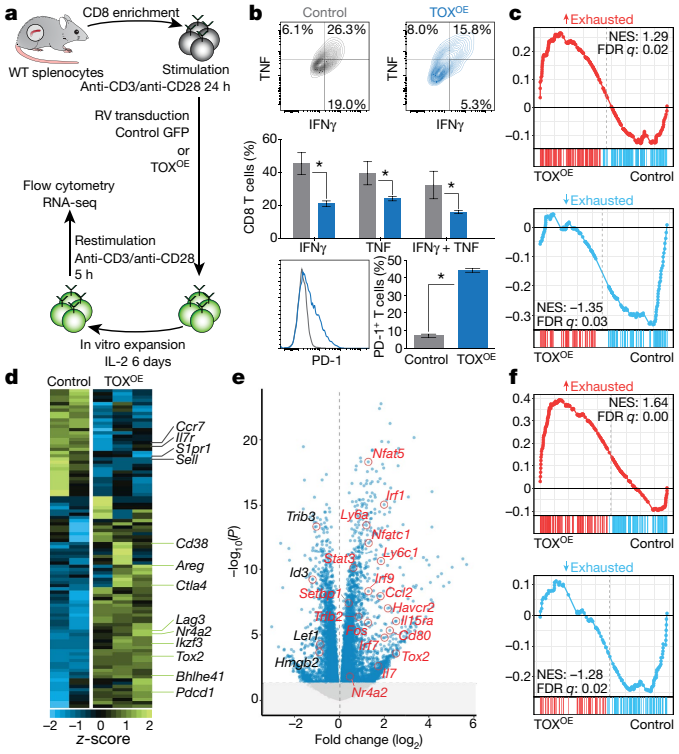

Fig. 5 | TOX enforces a T_{ex} cell transcriptional program. a, The experimental procedure used in **b**–**d**. $CD8^+$ T cells are isolated from spleens, activated, transduced with retroviruses encoding TOX (TOX^{OE}) or control GFP, and restimulated before analysis. **b**, The expression of cytokines and PD-1 after restimulation. **c**, Genes uniquely upregulated (red) or downregulated (blue) in T_{ex} cells[36] were assayed for enrichment in TOX^{OE} or control T cells using GSEA. **d**, Heat map of leading edge genes from **c**. Key genes associated with T_{ex} cells are labelled. **e**, Differentially expressed genes in TOX^{OE}-transduced relative to control-transduced fibroblasts. Transcripts with an FDR value of <0.05 are highlighted in blue. T_{ex}-associated genes from the leading edge of **f** labelled in red. **f**, As in **c**, genes uniquely upregulated (red) or downregulated (blue) in T_{ex} cells were analysed for enrichment in TOX^{OE}-transduced compared with control-transduced fibroblasts[36]. Contour and histogram plots are representative of at least three independent experiments. RNA sequencing datasets were generated from at least two biological replicates. Heat maps were generated using *z*-scores derived from $\log_2$ tag counts. Statistical significance ($^*P < 0.01$) was determined using the Student's *t*-test, error is reported as s.d.

which suggests that TOX represses the accessibility of genes involved in T_{eff} cell differentiation. By contrast, loci with reduced chromatin accessibility included *Tcf7* and other genes that are associated with T_{mem} and T_{ex} progenitors, including *Ccr7*, *Slamf6*, *Bach2* and *Ikzf2* (Fig. 6a, c, Extended Data Fig. 6c). Indeed, loci with significantly reduced chromatin accessibility in $Tox^{-/-}$ P14 T cells were highly enriched in T_{ex}-cell-specific sites (647/1,697; 38%), whereas sites with increased chromatin accessibility were enriched in T_{eff}-cell-specific sites (430/2,233; 19%) (Fig. 6d, Extended Data Fig. 6d). Globally, the epigenetic signature of TOX-deficient P14 T cells at day 8 of chronic infection was strongly enriched in the T_{eff} cell signature from acute infection and depleted in the T_{ex} cell epigenetic signature (Fig. 6e, Extended Data Fig. 6e). Moreover, specific peaks in the ATAC–seq profile were identified for key genes that changed in a TOX-dependent manner—including *Klrg1*, *Zeb2* and *Clnk*, which became more accessible in the absence of TOX, and *Tcf7*, *Bach2* and *Ikzf2*, for which the peaks were reduced or lost altogether (Fig. 6b, c, Extended Data Fig. 6b, c). Notably, the epigenetic changes caused by TOX corresponded to functionally relevant events, because there was a strong association of chromatin opening with increased gene expression and vice versa (Extended Data Fig. 6f). Thus, these data indicate a role for TOX in both the opening and closing of genomic regions associated with T_{ex} or T_{eff} cell differentiation, respectively.

We next examined epigenetic changes following the expression of TOX in isolated T cells from spleens (Fig. 5a). Retrovirus-mediated TOX expression induced chromatin accessibility changes in 378 sites (Fig. 6f, Extended Data Fig. 6a, Supplementary Table 6). These epigenetic changes strongly enriched for the landscape observed in in vivo T_{ex} cells, but also overlapped with the landscape found in T_{eff} cells, possibly reflecting activation aspects of this short-term in vitro assay or highlighting the common epigenetic module shared between T_{ex} and T_{eff} cells[13,14] (Fig. 6g, Extended Data Fig. 6g). Moreover, at least one region opened by TOX was the T_{ex}-cell-specific enhancer that is −23.8 kb upstream of the *Pdcd1* transcription start site, which indicates that at least some exhaustion-specific epigenetic changes can be induced in vitro by TOX[13,14] (Extended Data Fig. 6h).

To investigate the mechanism by which TOX induced T_{ex}-cell-related epigenetic changes, we identified proteins that were bound to TOX using immunoprecipitation followed by mass spectrometry (Extended Data Fig. 6i). Mass spectrometry identified proteins involved in chromatin organization and remodelling, RNA processing and translation, as well as DNA replication as TOX binding partners (Extended Data Fig. 6j, Supplementary Table 7). Network analysis identified the HBO1 complex, which is involved in the acetylation of histone H4 and H3, as a major set of TOX-bound proteins (Fig. 6h, i); indeed, four members of the histone H4-targeting HBO1 complex (KAT7, ING4, MEAF6 and JADE2) were identified by mass spectrometry[38,39] (Fig. 6h, i, Supplementary Table 7). Co-immunoprecipitation confirmed that TOX interacted with KAT7, the acetyl transferase component of the HBO1 complex[38,39] (Fig. 6j). TOX also bound proteins that are involved in repressive epigenetic events—including DNMT1, LEO1, PAF1, SAP130 and SIN3A—which indicates interactions with proteins that are involved in both the closing and the opening of chromatin (Fig. 6h, Supplementary Table 7). Thus, TOX can bind and probably recruit diverse sets of chromatin remodelling proteins.

Finally, we reasoned that TOX might modulate epigenetic accessibility and indirectly affect gene expression by altering the network of transcription factors and their targets in T_{ex} cells. PageRank network analysis[40] of transcriptional and epigenetic data revealed that $Tox^{-/-}$ T cells were negatively enriched in multiple transcription-factor networks downstream of TCR signalling (Fos, Jun, Stat, Batf families), including NFAT2 (Fig. 6k). Moreover, transcription-factor networks that are associated with transcriptional regulation (NR1D2, ATF3, BCL6 and SOX4) and the maintenance of cellular stemness (NANOG and SOX2)[41] were also lost in TOX-deficient T cells (Fig. 6k). Together, these data suggest a model in which TOX—working with other transcription factors—is central to an epigenetic and transcriptional regulatory cascade that orchestrates the development of T_{ex} cells.

Discussion

Here we demonstrate a major role for TOX as the key inducer of canonical features of T cell exhaustion and as an initiator of the T_{ex}-cell-specific epigenetic program. These findings have several potential implications. First, TOX expression and the molecular events that are controlled by TOX could aid in the more accurate detection, quantification and evaluation of T_{ex} cells. Notably, recent mass cytometry studies of human $CD8^+$ T cells found that TOX was expressed in the vast majority of T_{ex} cells from patients with HIV and lung cancer[36]. Second, these studies point to key molecular underpinnings of exhaustion that are relevant for reversibility and re-invigoration by immunotherapies, including PD-1/PD-L1 blockade[3,10,11,13,42–44]. TOX or TOX-dependent events—including epigenetic landscape programming—may be a major reason for this developmental inflexibility of T_{ex} cells even after PD-1 blockade[13], which suggests potential therapeutic strategies based on TOX manipulation. Finally, these data support the notion that T_{ex} cells are a distinct cell type from T_{eff} or T_{mem} cells[13–16] and provide a molecular mechanism for this divergent path of differentiation.

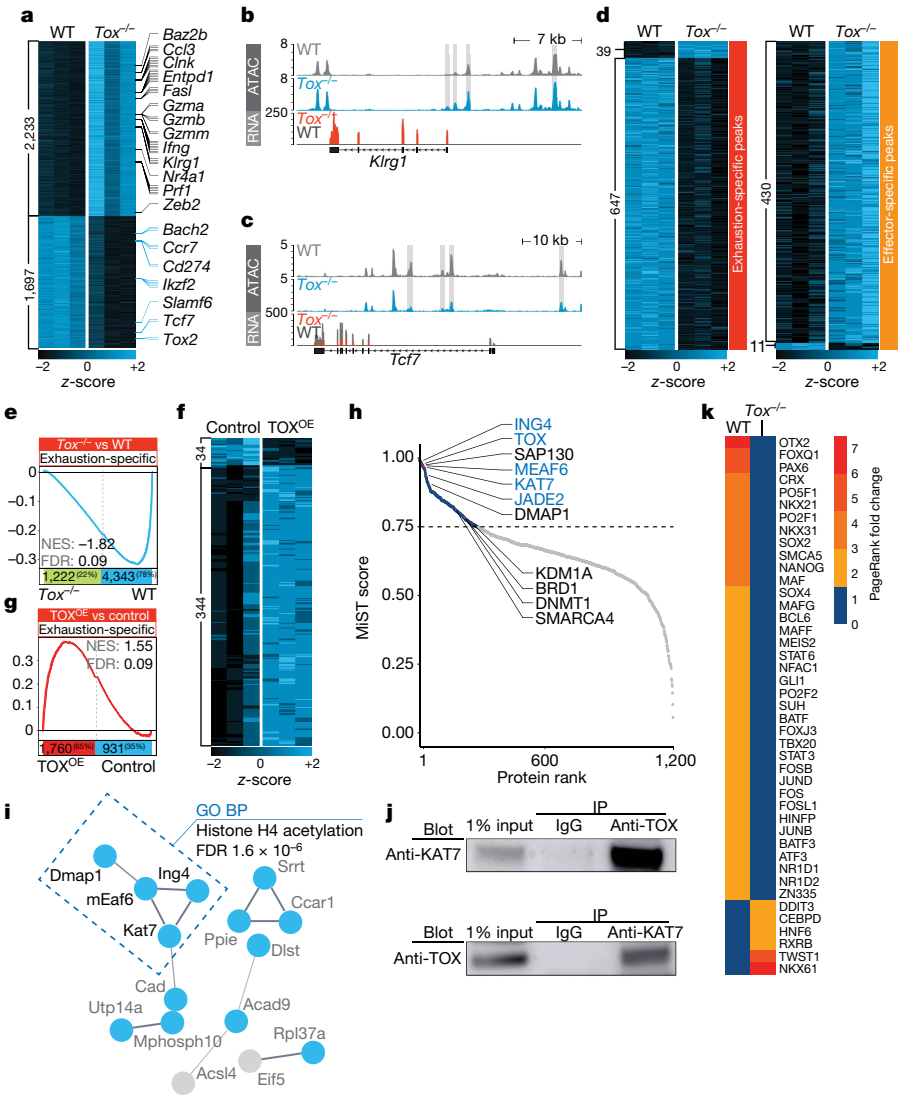

Fig. 6 | TOX induces an epigenetic signature of exhaustion in vitro and in vivo. a–e, ATAC–seq analysis of *Tox*$^{-/-}$ and wild-type P14 T cells after 8 days of clone-13 infection. **a**, Differentially accessible loci. Regions proximal to T_{eff} cells (black) and T_{mem} or naive T cells (blue) genes are labelled. The numbers on the left denote the number of gene-proximal loci with significant accessibility changes. Each column represents a biological replicate. **b**, **c**, ATAC–seq and RNA sequencing tracks of T_{eff}-cell-associated (**b**) or T_{mem}-cell-associated (**c**) loci. Differentially accessible sites are highlighted with grey bars. **d**, Significantly differentially accessible open chromatin regions (FDR < 0.05) in wild-type and *Tox*$^{-/-}$ T cells at T_{ex}-cell-specific and T_{eff}-cell-specific chromatin accessibility peaks[13]. **e**, Chromatin regions specifically accessible in T_{ex} cells[13] were analysed for enrichment in the *Tox*$^{-/-}$ versus wild-type P14 T cells by peak set enrichment analysis (PSEA). **f**, **g**, ATAC–seq analysis of in vitro T cells transduced with a retrovirus encoding TOX (TOX^{OE}) or control GFP. **f**, Differentially accessible chromatin regions in TOX^{OE} compared to control cells. **g**, PSEA of T_{ex}-cell-specific loci as in **e** using differentially accessible loci in TOX^{OE} versus control CD8$^+$ T cells. **h**, MiST (mass spectrometry interaction statistics) score of proteins identified after TOX immunoprecipitation and mass spectrometry from EL4 lysate. The dashed line indicates high-confidence hits. **i**, STRING network analysis of proteins with a MiST score of >0.90. Gene ontology biological process (GO BP) analysis on a subsequent network is highlighted. **j**, Top, anti-TOX was used for the immunoprecipitation of TOX from EL4 lysate and blotted with anti-KAT7. Bottom, reverse immunoprecipitation was performed by immunoprecipitating with anti-KAT7, then blotting with anti-TOX. **k**, Heat map of transcription factors for which the PageRank score shows a difference of greater than 1.5-fold between wild-type and *Tox*$^{-/-}$ P14 T cells on day 8 of clone-13 infection. NFAC1 represents NFAT2. Heat maps were generated using *z*-scores derived from $\log_2$ tag counts.

Our observations suggest a model in which TOX is a primary regulator of T_{ex} cells, similar to other developmental programmers in immune cells[45–48]. Collectively, these data demonstrate that TOX is required for the development of T_{ex} cells, although other transcription factors are clearly also involved. The identification of an epigenetic programming mechanism for T_{ex} cells also suggests new therapeutic possibilities based on the modulation of TOX and/or the TOX-dependent epigenetic changes in T_{ex} cells.

Online content

Any methods, additional references, Nature Research reporting summaries, source data, extended data, supplementary information, acknowledgements, peer review information; details of author contributions and competing interests; and statements of data and code availability are available at https://doi.org/10.1038/s41586-019-1325-x.

Received: 4 June 2018; Accepted: 30 May 2019;
Published online 17 June 2019.

1. Kaech, S. M. & Cui, W. Transcriptional control of effector and memory CD8$^+$ T cell differentiation. *Nat. Rev. Immunol.* **12**, 749–761 (2012).
2. Wherry, E. J. & Kurachi, M. Molecular and cellular insights into T cell exhaustion. *Nat. Rev. Immunol.* **15**, 486–499 (2015).
3. Barber, D. L. et al. Restoring function in exhausted CD8 T cells during chronic viral infection. *Nature* **439**, 682–687 (2006).
4. Frebel, H. et al. Programmed death 1 protects from fatal circulatory failure during systemic virus infection of mice. *J. Exp. Med.* **209**, 2485–2499 (2012).
5. Zajac, A. J. et al. Viral immune evasion due to persistence of activated T cells without effector function. *J. Exp. Med.* **188**, 2205–2213 (1998).

6. Gallimore, A. et al. Induction and exhaustion of lymphocytic choriomeningitis virus-specific cytotoxic T lymphocytes visualized using soluble tetrameric major histocompatibility complex class I-peptide complexes. *J. Exp. Med.* **187**, 1383–1393 (1998).
7. Lechner, F. et al. Analysis of successful immune responses in persons infected with hepatitis C virus. *J. Exp. Med.* **191**, 1499–1512 (2000).
8. Shankar, P. et al. Impaired function of circulating HIV-specific CD8$^+$ T cells in chronic human immunodeficiency virus infection. *Blood* **96**, 3094–3101 (2000).
9. Pauken, K. E. & Wherry, E. J. Overcoming T cell exhaustion in infection and cancer. *Trends Immunol.* **36**, 265–276 (2015).
10. Page, D. B., Postow, M. A., Callahan, M. K., Allison, J. P. & Wolchok, J. D. Immune modulation in cancer with antibodies. *Annu. Rev. Med.* **65**, 185–202 (2014).
11. Hirano, F. et al. Blockade of B7-H1 and PD-1 by monoclonal antibodies potentiates cancer therapeutic immunity. *Cancer Res.* **65**, 1089–1096 (2005).
12. Doering, T. A. et al. Network analysis reveals centrally connected genes and pathways involved in CD8$^+$ T cell exhaustion versus memory. *Immunity* **37**, 1130–1144 (2012).
13. Pauken, K. E. et al. Epigenetic stability of exhausted T cells limits durability of reinvigoration by PD-1 blockade. *Science* **354**, 1160–1165 (2016).
14. Sen, D. R. et al. The epigenetic landscape of T cell exhaustion. *Science* **354**, 1165–1169 (2016).
15. Scott-Browne, J. P. et al. Dynamic changes in chromatin accessibility occur in CD8$^+$ T cells responding to viral infection. *Immunity* **45**, 1327–1340 (2016).
16. Philip, M. et al. Chromatin states define tumour-specific T cell dysfunction and reprogramming. *Nature* **545**, 452–456 (2017).
17. Lara-Astiaso, D. et al. Chromatin state dynamics during blood formation. *Science* **345**, 943–949 (2014).
18. Carty, S. A. et al. The loss of TET2 promotes CD8$^+$ T cell memory differentiation. *J. Immunol.* **200**, 82–91 (2018).
19. Ghoneim, H. E. et al. De novo epigenetic programs inhibit PD-1 blockade-mediated T cell rejuvenation. *Cell* **170**, 142–157 (2017).
20. Aliahmad, P., Seksenyan, A. & Kaye, J. The many roles of TOX in the immune system. *Curr. Opin. Immunol.* **24**, 173–177 (2012).
21. Seehus, C. R. et al. The development of innate lymphoid cells requires TOX-dependent generation of a common innate lymphoid cell progenitor. *Nat. Immunol.* **16**, 599–608 (2015).
22. Whyte, W. A. et al. Master transcription factors and mediator establish super-enhancers at key cell identity genes. *Cell* **153**, 307–319 (2013).
23. Hnisz, D. et al. Super-enhancers in the control of cell identity and disease. *Cell* **155**, 934–947 (2013).
24. Wherry, E. J., Blattman, J. N., Murali-Krishna, K., van der Most, R. & Ahmed, R. Viral persistence alters CD8 T-cell immunodominance and tissue distribution and results in distinct stages of functional impairment. *J. Virol.* **77**, 4911–4927 (2003).
25. Joshi, N. S. et al. Inflammation directs memory precursor and short-lived effector CD8$^+$ T cell fates via the graded expression of T-bet transcription factor. *Immunity* **27**, 281–295 (2007).
26. Herndler-Brandstetter, D. et al. KLRG1$^+$ effector CD8$^+$ T cells lose KLRG1, differentiate into all memory T cell lineages, and convey enhanced protective immunity. *Immunity* **48**, 716–729 (2018).
27. Angelosanto, J. M., Blackburn, S. D., Crawford, A. & Wherry, E. J. Progressive loss of memory T cell potential and commitment to exhaustion during chronic viral infection. *J. Virol.* **86**, 8161–8170 (2012).
28. Paley, M. A. et al. Progenitor and terminal subsets of CD8$^+$ T cells cooperate to contain chronic viral infection. *Science* **338**, 1220–1225 (2012).
29. Utzschneider, D. T. et al. T cell factor 1-expressing memory-like CD8$^+$ T cells sustain the immune response to chronic viral infections. *Immunity* **45**, 415–427 (2016).
30. Wu, T. et al. The TCF1–Bcl6 axis counteracts type I interferon to repress exhaustion and maintain T cell stemness. *Sci. Immunol.* **1**, eaai8593 (2016).
31. Aliahmad, P. et al. TOX provides a link between calcineurin activation and CD8 lineage commitment. *J. Exp. Med.* **199**, 1089–1099 (2004).
32. Macian, F. NFAT proteins: key regulators of T-cell development and function. *Nat. Rev. Immunol.* **5**, 472–484 (2005).
33. Martinez, G. J. et al. The transcription factor NFAT promotes exhaustion of activated CD8$^+$ T cells. *Immunity* **42**, 265–278 (2015).
34. Klein-Hessling, S. et al. NFATc1 controls the cytotoxicity of CD8$^+$ T cells. *Nat. Commun.* **8**, 511 (2017).
35. Monticelli, S. & Rao, A. NFAT1 and NFAT2 are positive regulators of *IL-4* gene transcription. *Eur. J. Immunol.* **32**, 2971–2978 (2002).
36. Bengsch, B. et al. Epigenomic-guided mass cytometry profiling reveals disease-specific features of exhausted CD8 T cells. *Immunity* **48**, 1029–1045 (2018).
37. Johnson, J. L. et al. Lineage-determining transcription factor TCF-1 initiates the epigenetic identity of T cells. *Immunity* **48**, 243–257 (2018).
38. Lalonde, M. E. et al. Exchange of associated factors directs a switch in HBO1 acetyltransferase histone tail specificity. *Genes Dev.* **27**, 2009–2024 (2013).
39. Miotto, B. & Struhl, K. HBO1 histone acetylase activity is essential for DNA replication licensing and inhibited by Geminin. *Mol. Cell* **37**, 57–66 (2010).
40. Yu, B. et al. Epigenetic landscapes reveal transcription factors that regulate CD8$^+$ T cell differentiation. *Nat. Immunol.* **18**, 573–582 (2017).
41. Boiani, M. & Schöler, H. R. Regulatory networks in embryo-derived pluripotent stem cells. *Nat. Rev. Mol. Cell Biol.* **6**, 872–881 (2005).
42. Iwai, Y., Terawaki, S. & Honjo, T. PD-1 blockade inhibits hematogenous spread of poorly immunogenic tumor cells by enhanced recruitment of effector T cells. *Int. Immunol.* **17**, 133–144 (2005).
43. Strome, S. E. et al. B7-H1 blockade augments adoptive T-cell immunotherapy for squamous cell carcinoma. *Cancer Res.* **63**, 6501–6505 (2003).
44. Blank, C. et al. PD-L1/B7H-1 inhibits the effector phase of tumor rejection by T cell receptor (TCR) transgenic CD8$^+$ T cells. *Cancer Res.* **64**, 1140–1145 (2004).
45. Anderson, K. L. et al. Transcription factor PU.1 is necessary for development of thymic and myeloid progenitor-derived dendritic cells. *J. Immunol.* **164**, 1855–1861 (2000).
46. Fontenot, J. D., Gavin, M. A. & Rudensky, A. Y. Foxp3 programs the development and function of CD4$^+$CD25$^+$ regulatory T cells. *Nat. Immunol.* **4**, 330–336 (2003).
47. Hori, S., Nomura, T. & Sakaguchi, S. Control of regulatory T cell development by the transcription factor Foxp3. *Science* **299**, 1057–1061 (2003).
48. Weber, B. N. et al. A critical role for TCF-1 in T-lineage specification and differentiation. *Nature* **476**, 63–68 (2011).

METHODS

Data reporting. No statistical methods were used to predetermine sample size. The experiments were not randomized and the investigators were not blinded to allocation during experiments and outcome assessment.

Mice. Mice were maintained in a specific-pathogen-free facility at the University of Pennsylvania (UPenn). Experiments and procedures were performed in accordance with the Institutional Animal Care and Use Committee (IACUC) of UPenn. Mice of the following genotypes were on a C57BL/6J background and bred at UPenn or purchased from Jackson Laboratory: wild-type P14, *Tox*$^{flox/flox}$*Cd4*^{cre} P14, *Tox*$^{-/-}$ P14 and *Nfatc1*$^{flox/flox}$*Cd4*^{cre} P14. *Tox*$^{flox/flox}$ and *Tox*$^{-/-}$ mice were provided by J. Kaye[49]. For experiments with CT26 tumours, BALB/c mice from Charles River were used. For all experiments mice were age- and sex-matched and male and female mice between 6–8 weeks of age were randomly assigned to experimental groups.

Naive lymphocyte isolation and adoptive T cell transfer. T cell receptor transgenic GP33-specific CD8$^+$ T cells (P14) were isolated from the peripheral blood of donor mice using gradient centrifugation with Histopaque-1083 (Sigma-Aldrich). For experiments using LCMV infection, wild-type P14 T cells were mixed 1:1 with congenically disparate P14 T cells of the desired genotype (*Tox*$^{flox/flox}$*Cd4*^{cre} P14, *Tox*$^{-/-}$ P14, or *Nfatc1*$^{flox/flox}$*Cd4*^{cre} P14) and a total of 500 naive cells were adoptively transferred by tail-vein injection into 6–8-week-old recipient mice 1–5 days before infection. Recipients were of a third congenic background to enable us to distinguish both donor populations from the host T cells. Naive wild-type and TOX cKO P14 T cells had similar baseline activation and expression of inhibitory receptors, enabling a direct comparison (Extended Data Fig. 3b). For experiments that monitored only wild-type P14 responses, 500 cells were transferred. Previous reports have shown that adoptive transfer of 500 P14 T cells before infection with LCMV clone 13 or Armstrong does not affect viral load or pathogenesis[4,50,51]. For LCMV experiments, mice were not depleted of CD4$^+$ T cells using GK1.5 antibody before infection. For experiments with influenza, *Listeria monocytogenes* or vesicular stomatitis virus infection (VSV), 5,000 P14 T cells (influenza, *L. monocytogenes*) or OT-I (VSV) CD8$^+$ T cells were adoptively transferred before infection.

Viral infections, bacterial infections, and treatments. LCMV strains Armstrong and clone 13 were propagated and titres were determined as previously described[51]. C57BL/6J mice were infected intraperitoneally with 2×10^5 plaque-forming units (PFU) of LCMV Armstrong or intravenously with 4×10^6 PFU LCMV clone 13. For other experiments, mice were infected with 2×10^6 PFU VSV-OVA (intravenously) or 1×10^4 colony-forming units (CFU) *L. monocytogenes* GP33 intraperitoneally. For influenza infection, mice were anaesthetized with isofluorane and ketamine before intranasal administration of 50 $TCID_{50}$ PR8-GP33 (H1N1 strain) in 30 μl of PBS. FK506 (Prograf, Astellas Pharma) was prepared for injection by diluting to 1.5 mg ml^{-1} in PBS. Diluted FK506 was administered subcutaneously at a dose of 10 mg kg^{-1} from day 3–7 or day 25–29 of LCMV clone-13 infection[52]. Cyclosporin A (Sigma-Aldrich) was prepared by dilution in sunflower oil (Sigma-Aldrich). A diluted solution (40 mg kg^{-1}) was administered intraperitoneally each day for the duration of treatment. For control treatments, PBS was administered subcutaneously.

Retroviral transduction, in vitro differentiation and cell transfer. For retroviral transduction, CD8$^+$ T cells were enriched from the spleens of donor mice using an EasySep magnetic negative selection kit (Stem Cell Technologies) and transduced as described previously[53]. In brief, cells were resuspended at 10^6 per ml in complete RPMI (cRPMI): RPMI 1640 supplemented with 10% FBS, 50 μM β-mercaptoethanol, 100 U ml^{-1} penicillin, 100 U ml^{-1} streptomycin, non-essential amino acids (Invitrogen), sodium pyruvate (Invitrogen) and HEPES buffer (Invitrogen). T cells (3×10^6) were plated in wells of a 12-well cluster dish and activated for 18–24 h with 1 μg ml^{-1} anti-CD3ε (145-2C11, BioLegend) and 0.5 μg ml^{-1} anti-CD28 (37.51, BioLegend) antibodies in the presence of 100 U ml^{-1} recombinant human IL-2 (Peprotech). After activation, cells were resuspended at 3×10^6 per ml in cRPMI, plated in a well of a six-well plate and transduced with MigR1-based retroviruses in the presence of polybrene (4 μg ml^{-1}) by spin infection (2,000*g* for 75 min at 32 °C). Retroviral supernatants were produced by co-transfecting HEK293T cells with a retrovirus expression plasmid and a pCL-Eco packaging plasmid using Lipofectamine 3000 (Invitrogen).

For in vitro experiments, transduced T cells were expanded and differentiated into effector T cells[33] by culturing in cRPMI in the presence of IL-2 (100 U ml^{-1}) for 5 additional days. Restimulations were performed by incubating cells with biotinylated anti-CD3ε (1 μg ml^{-1}, 145-2C11, BioLegend) and anti-CD28 (0.5 μg ml^{-1}, 37.51, BioLegend) antibodies for 5 min followed by the addition of 25 μg ml^{-1} streptavidin (Invitrogen) for 5 h in a 37 °C incubator.

For experiments involving the transfer of transduced P14 T cells into mice, the mice were infected with LCMV Armstrong or clone 13 on the same day as transduction. Twenty-four hours after transduction, GFP$^+$ cells were sorted to >98% purity and transferred intravenously into infected hosts.

Ectopic tumour models, cell transfers and area measurements. B16-F10, B16-F10-GP33 melanoma, and CT26 colon carcinoma cell lines were purchased from ATCC. Tumour cells were maintained at 37 °C in DMEM medium supplemented with 10% FBS, 100 U ml^{-1} penicillin, 100 U ml^{-1} streptomycin and 2 mM L-glutamine. Tumour cells (2×10^5) were injected subcutaneously into the flanks of mice. To measure antigen-specific T cell responses, P14 T cells were isolated from spleens of naive mice and activated as described above for retrovirus transduction. Activated cells were passaged every 24 h and plated at 3×10^6 in 3 ml cRPMI with 100 U ml^{-1} recombinant human IL-2 per well of a six-well plate. Seventy-two hours after activation, 1×10^6 cells were transferred intravenously per tumour-inoculated mouse. T cell transfers were performed 5 days after tumour inoculation. Tumour size was measured using digital calipers every 48 h after inoculation.

Plasmids and cloning. Retroviral vectors encoding TOX were generated by first amplifying Gateway cloning compatible inserts from an ORF clone (Origene MR208435). PCR products were purified (PCR Purification Kit, Qiagen) and subcloned into pDONR221 using BP clonase (Invitrogen) following the manufacturer's instructions. Entry clones were subsequently cloned into a Gateway-compatible MigR1 vector using LR clonase (Invitrogen). Wild-type-NFAT2 and CA-NFAT2 retrovirus plasmids were gifts from A. Rao (Addgene plasmids 11101 and 11102).

Preparation of cell suspensions and restimulations. After infection or tumour challenge, CD8$^+$ T cells were isolated from spleen and draining lymph nodes by cutting samples into small pieces and homogenizing against a 70-μm cell strainer. Cells were run through the cell strainer and red blood cells were lysed in ACK lysis buffer (Thermo Fisher Scientific) for 5 min. The cell suspension was then washed in PBS and passed through a 70-μm cell strainer once more. Lungs and tumours were cut into small pieces using surgical scissors and digested for 1 h at 37 °C in RPMI 1640 medium supplemented with 5% FBS, 100 U ml^{-1} DNaseI (Sigma-Aldrich) and 0.2 mg ml^{-1} collagenase IV (Sigma-Aldrich). Samples were subsequently mechanically disrupted against a 70-μm filter and washed with PBS. Red blood cells were lysed in ACK lysis buffer for 5 min and samples were re-filtered through a 70-μm strainer. To assess cytokine and effector molecule production, 2×10^6 cells were plated in 200 μl cRPMI in wells of a flat-bottom 96-well dish and incubated with GP33 peptide in the presence of protein transport inhibitors (GolgiStop and GolgiPlug, BD Biosciences) for 5 h at 37 °C.

Human sample collection and staining. Normal donor peripheral blood samples ($n = 10$, male and female donors, aged 18–39) were obtained from Cellular Technology. Human melanoma tumour and peripheral blood mononuclear cell samples were collected from patients with stage III and stage IV melanoma under the University of Pennsylvania Abramson Cancer Center's melanoma research program tissue collection protocol UPCC 08607 and IRB 703001 in accordance with the Institutional Review Board. Tumour samples were procured from the operating room and processed the same day using manual dissociation into a single-cell suspension. Tumour samples were then frozen immediately using standard freezing media, and stored in liquid nitrogen. All human samples were processed and stained as previously described[54].

Flow cytometry and cell sorting. Antibodies were procured from the following sources: BioLegend: CD44 (IM7), CD62L (MEL-14), CD127 (A7R34), T-bet (4B10), PD-1 (RMP1-30), CD160 (7H1), TIM-3 (RMT3-23), CD3ε (17A2), TNF (MP6-XT22), CD8α (53-6.7), CD4 (RM4-5), CD45.1 (A29), CD45.2 (104); Miltenyi Biotec: TOX (REA473); Southern Biotech: KLRG1 (2F1); eBioscience: Eomes (Dan11mag), 2B4 (eBio244F4), IFNγ (XMG1.2), granzyme B (GB11), B220 (RA3-6B2); BD Biosciences: TIGIT (1G9), LAG-3 (C9B7W), TCF-1 (S33-966), 2B4 (2B4), Ki-67 (B56). Live cells were discriminated by staining with Zombie NIR dye (BioLegend). Intracellular and nuclear staining of cytokines, effector molecules and transcription factors was performed using the FoxP3/Transcription Factor Staining Buffer Set (eBioscience) in accordance with the manufacturer's protocol. Flow cytometry data were acquired on a BD LSR II instrument and cell sorting was performed on a BD FACSAria enclosed within a laminar flow hood. Data were analysed using FlowJo software (TreeStar).

Microarray analysis. Microarray data (GSE41867)[12] were processed as previously described[12,13]. Genes with chromatin-modulating function were identified by compiling gene lists retrieved from gene ontology associations (GO molecular functions: chromatin binding, nucleic-acid binding, nucleotide binding; and PANTHER protein classes: DNA-binding protein, chromatin-binding protein), the EpiFactors database[55] and previously identified chromatin modulators[56] (Supplementary Table 9).

RNA-seq and ATAC–seq sample preparation and sequencing. To assess the transcriptional and epigenetic effect of TOX deletion in T cells, 250 wild-type and 250 *Tox*$^{-/-}$ naive CD44^{low}CD62L^{high} P14 T cells sorted from peripheral blood of donors, mixed and co-transferred into wild-type mice. Recipients were subsequently infected with LCMV clone 13 and splenocytes were collected 8 days after infection. Ten spleens were pooled for each of the three replicates before processing, CD8$^+$ T cell enrichment (using EasySep CD8$^+$ T cell negative selection

kit, Stem Cell Technologies), and staining of single-cell suspensions. Wild-type and TOX-deficient P14 T cells (1×10^5) were sorted to a purity of >98% for each replicate. In ectopic and enforced expression experiments, in vitro differentiated $CD8^+$ T cells transduced with TOX + GFP or control GFP only (>2 biological replicates each) were sorted on GFP expression 6 days after initial activation to a purity of >98%. NIH3T3 cells were transduced with TOX + GFP or control GFP-only retroviruses and cultured for 48 h before cell sorting. To extract RNA, 50,000 cells were resuspended in RLT buffer supplemented with β-mercaptoethanol and processed with a RNeasy Micro Kit (Qiagen) as per the manufacturer's instructions. Total RNA libraries were prepared using a Pico Input SMARTer Stranded Total RNA-Seq Kit (Takara). Extracted RNA and libraries were assessed for quality on a TapeStation 2200 instrument (Agilent). ATAC libraries were generated as described with minor modifications[57]. In brief, nuclei from 50,000 cells were isolated using a lysis solution composed of 10 mM Tris-HCl, 10 mM NaCl, 3 mM $MgCl_2$, and 0.1% IGEPAL CA-630. Immediately after cell lysis, nuclei were pelleted in low-bind 1.5-ml tubes (Eppendorf) and resuspended in TD buffer with Tn5 transposase (Illumina). The transposition reaction was performed at 37 °C for 45 min. DNA fragments were purified from enzyme solution using MinElute Enzyme Reaction Cleanup Kit (Qiagen). Libraries were barcoded (Nextera Index Kit, Illumina) and amplified with NEBNext High Fidelity PCR Mix (New England Biolabs). Library quality was assessed using a TapeStation instrument. RNA and ATAC libraries were quantified using a KAPA Library Quantification Kit and sequenced on an Illumina NextSeq 550 instrument (150 bp, paired-end) on high-output flow cells.

RNA-seq data processing and analysis. FASTQ files were aligned using STAR 2.5.2a against the mm10 mouse reference genome. The aligned files were processed using PORT gene-based normalization (https://github.com/itmat/Normalization). Differential gene expression was performed with Limma. Limma-voom was used to identify transcripts that were significantly differentially expressed between experimental groups using an adjusted *P* value of <0.05.

ATAC–seq data processing and analysis. The script used for processing raw ATAC–seq FASTQ data are available at the following GitHub repository: https://github.com/wherrylab/jogiles_ATAC. In brief, samples were aligned to the mm10 reference genome with Bowtie2. Unmapped, unpaired and mitochrondrial reads were removed using samtools. ENCODE Blacklist regions were removed (https://sites.google.com/site/anshulkundaje/projects/blacklists). PCR duplicates were removed using Picard. Peak calling was performed with MACS2 with a FDR *q*-value of 0.01. A union peak list for each experiment was created by combining all peaks in all samples; overlapping peaks were merged using bedtools merge. The number of reads in each peak was determined with bedtools coverage. Differentially expressed peaks were identified after DESeq2 normalization using a FDR cut-off of <0.05.

Super enhancers were identified by running the ROSE algorithm (https://bitbucket.org/young_computation/rose) on normalized ATAC–seq data previously generated from naive, effector, memory or exhausted $CD8^+$ T cells[13]. The stitching distance was set to 12.5 kb and transcription-start-site exclusion to 2.5 kb.

The scripts for peak set enrichment are available at https://github.com/wherrylab/jogiles_ATAC. In brief, bedtools intersect was used to find overlapping peaks between the experiment and the peak set of interest. Peak names between the experiment and peak set of interest were unified using custom R scripts. GSEA was used to calculate enrichment scores.

Taiji/PageRank network analysis. The Taiji pipeline integrates diverse datasets to identify master regulators, including genome-wide expression profile and chromatin state. Analysis was performed on RNA-seq and ATAC–seq data generated from wild-type and $Tox^{-/-}$ P14 T cells after 8 days of infection with clone 13 (as described in Figs. 3 and 6, respectively). Herein, we implemented the pipeline described previously (http://wanglab.ucsd.edu/star/taiji)[40]. In brief, ATAC–seq peaks were called by MACS2 v.2.1.1 to annotate genome-wide regulatory elements and the regulatory elements are assigned to their nearest genes. Known transcription-factor motifs are scanned in the open chromatin region within each regulatory element to pinpoint the putative binding-sites. Transcription factors with putative binding-sites in promoters or enhancers are then linked to their target genes to form a network. As part of Taiji pagerank analysis, a personalized PageRank algorithm is used to assess the importance of transcription factors in the network and ranks are calculated for each transcription factor on the basis of epigenetic and RNA expression data. The normalized ranks are then compared across conditions by calculating fold change and the top transcription factors are chosen using a cut-off of 1.5× above the mean. These transcription factors are finally visualized in a heat map.

Immunoprecipitation and immunoblotting. Immunoprecipitation was performed as previously described[58]. In brief, 5×10^6 EL4 cells were lysed in immunoprecipitation buffer (20 mM Tris, pH 7.5, 137 mM NaCl, 1 mM $MgCl_2$, 1 mM $CaCl_2$, 1% NP-40, 10% glycerol) supplemented with 1:100 HALT protease and phosphatase inhibitor cocktail (Thermo Scientific) and benzonase (Novagen) at 12.5 U ml^{-1}. Lysates were rotated at 4 °C for 60 min. Subsequently, antibody-conjugated Dynabeads (Invitrogen) were added and samples were incubated at 4 °C overnight on a rotating platform. Beads were collected using a magnet and samples were washed five times with immunoprecipitation buffer. Samples were then resuspended in NuPAGE loading dye (Thermo Fisher), incubated at 95 °C for 5 min and analysed by western blotting. The following antibodies were used for immunoprecipitation: TOX (ab155768, Abcam) and KAT7 (ab70183, Abcam); and for western blot: TOX (TXRX10, eBioscience), KAT7 (ab70183, Abcam), H3K4me1 (ab8895, Abcam), H3K27me3 (ab6002, Abcam), H3K9ac (39918, Active Motif), H3K27ac (ab4729, Abcam), H4 (07-108, Millipore) and H4ac (06-866, Millipore).

Immunoprecipitation, LC–MS/MS and analysis. We used EL4 thymoma cells that express high levels of TOX and have been used previously to model some features of T_{ex} cells[14]. EL4 cell nuclear extract was prepared as described[59]. In brief, cells were incubated in hypotonic buffer (10 mM Tris-Cl, pH 7.4, 1.5 mM $MgCl_2$, 10 mM KCl, 25 mM NaF, 1 mM Na_3VO_4, 1 mM dithiothreitol (DTT) and Roche protease inhibitor cocktail) for 3 min. Cell pellets were subsequently spun down, resuspended in hypotonic buffer, and homogenized with five strokes of a Dounce homogenizer. Nuclei were collected by centrifugation and resuspended in extraction buffer (50 mM Tris-Cl, pH 7.4, 1.5 mM $MgCl_2$, 20% glycerol, 420 mM NaCl, 25 mM NaF, 1 mM Na_3VO_4, 1 mM DTT, 400 U ml^{-1} DNase I and protease inhibitor cocktail). Samples were incubated for 30 min at 4 °C on a rotating plat form. Extracts were diluted 3:1 in buffer containing 50 mM Tris-Cl, pH 7.4, 1.5 mM $MgCl_2$, 25 mM NaF, 1 mM Na_3VO_4, 0.6% NP-40, 1 mM DTT and protease inhibitor cocktail. Immunopurification was carried out on 1 mg of nuclear extract using a magnetic co-immunoprecipitation kit (Thermo Fisher) with 40 μg anti-TOX (Abcam, ab155768) or control IgG antibody as per the manufacturer's instructions.

Liquid chromatography coupled with tandem mass spectrometry (LC–MS/MS) analysis was performed by the Proteomics and Metabolomics Facility at the Wistar Institute using a Q Exactive Plus mass spectrometer (Thermo Fisher) coupled with a Nano-ACQUITY UPLC system (Waters). Samples were digested in-gel with trypsin and injected onto a UPLC Symmetry trap column (180 μm i.d. × 2 cm packed with 5 μm C18 resin; Waters). Tryptic peptides were separated by reversed-phase HPLC on a BEH C18 nanocapillary analytical column (75 μm i.d. × 25 cm, 1.7 μm particle size; Waters) using a 95 min gradient formed by solvent A (0.1% formic acid in water) and solvent B (0.1% formic acid in acetonitrile). A 30-min blank gradient was run between sample injections to minimize carryover. Eluted peptides were analysed by the mass spectrometer set to repetitively scan *m*/*z* from 400 to 2,000 in positive-ion mode. The full MS scan was collected at 70,000 resolution followed by data-dependent MS/MS scans at 17,500 resolution on the 20 most abundant ions exceeding a minimum threshold of 20,000. Peptide match was set as preferred, exclude isotopes option and charge-state screening were enabled to reject singly and unassigned charged ions. Peptide sequences were identified using MaxQuant 1.5.2.8. MS/MS spectra were searched against a UniProt human protein database using full tryptic specificity with up to two missed cleavages, static carboxamidomethylation of Cys, and variable oxidation of Met and protein N-terminal acetylation. Consensus identification lists were generated with FDRs of 1% at protein and peptide levels. To generate a list of statistically significant hits, the resulting iBAQ protein values from the MaxQuant output were analysed using the MiST scoring system[60], which accounts for protein abundance, specificity and reproducibility across three biological replicates. STRING protein–protein network analysis was performed on proteins with a MiST score of >0.90 using an interaction score of 0.4 (medium).

Statistical analysis. Statistical tests for flow-cytometry data were performed using GraphPad Prism software. A *P* value of <0.05 was considered significant in these analyses. A Student's *t*-test (two-tailed) was used for comparisons between two independent conditions. A paired Student's *t*-test was used when the samples being compared originated from the same mouse.

Reporting summary. Further information on research design is available in the Nature Research Reporting Summary linked to this paper.

Data availability

RNA-seq and ATAC–seq data have been deposited in the NCBI Gene Expression Omnibus (GEO) database and are accessible through the GEO SuperSeries accession number: GSE131871. All other relevant data are available from the corresponding author upon reasonable request.

Code availability

Custom code used for RNA-seq and ATAC–seq analyses are available at the GitHub links provided above.

49. Aliahmad, P. & Kaye, J. Development of all CD4 T lineages requires nuclear factor TOX. *J. Exp. Med.* **205**, 245–256 (2008).

50. Blattman, J. N., Wherry, E. J., Ha, S. J., van der Most, R. G. & Ahmed, R. Impact of epitope escape on PD-1 expression and CD8 T-cell exhaustion during chronic infection. *J. Virol.* **83**, 4386–4394 (2009).
51. Odorizzi, P. M., Pauken, K. E., Paley, M. A., Sharpe, A. & Wherry, E. J. Genetic absence of PD-1 promotes accumulation of terminally differentiated exhausted $CD8^+$ T cells. *J. Exp. Med.* **212**, 1125–1137 (2015).
52. Araki, K. et al. Pathogenic virus-specific T cells cause disease during treatment with the calcineurin inhibitor FK506: implications for transplantation. *J. Exp. Med.* **207**, 2355–2367 (2010).
53. Kurachi, M. et al. Optimized retroviral transduction of mouse T cells for in vivo assessment of gene function. *Nat. Protoc.* **12**, 1980–1998 (2017).
54. Huang, A. C. et al. T-cell invigoration to tumour burden ratio associated with anti-PD-1 response. *Nature* **545**, 60–65 (2017).
55. Medvedeva, Y. A. et al. EpiFactors: a comprehensive database of human epigenetic factors and complexes. *Database (Oxford)* **2015**, bav067 (2015).
56. Shi, J. et al. Discovery of cancer drug targets by CRISPR–Cas9 screening of protein domains. *Nat. Biotechnol.* **33**, 661–667 (2015).
57. Buenrostro, J. D., Giresi, P. G., Zaba, L. C., Chang, H. Y. & Greenleaf, W. J. Transposition of native chromatin for fast and sensitive epigenomic profiling of open chromatin, DNA-binding proteins and nucleosome position. *Nat. Methods* **10**, 1213–1218 (2013).
58. Dou, Z. et al. Autophagy mediates degradation of nuclear lamina. *Nature* **527**, 105–109 (2015).
59. Dawson, M. A. et al. Inhibition of BET recruitment to chromatin as an effective treatment for MLL-fusion leukaemia. *Nature* **478**, 529–533 (2011).
60. Jäger, S. et al. Global landscape of HIV–human protein complexes. *Nature* **481**, 365–370 (2012).
61. Guo, X. et al. Global characterization of T cells in non-small-cell lung cancer by single-cell sequencing. *Nat. Med.* **24**, 978–985 (2018).
62. Zheng, C. et al. Landscape of infiltrating T cells in liver cancer revealed by single-cell sequencing. *Cell* **169**, 1342–1356 (2017).

Acknowledgements We thank all members of the Wherry laboratory for helpful discussions and critical analysis of the manuscript; J. Kaye for providing the $Tox^{flox/flox}$ and $Tox^{-/-}$ mice; P. M. Porrett for providing FK506; D. Zehn and A. Schietinger for helpful discussions; and H.-Y. Tang and T. Beer of the Wistar Institute Proteomics and Metabolomics Facility for assistance with the analysis of the proteomics data. Support for the Wistar Proteomics and Metabolomics Core Facility was provided by Cancer Center Support Grant CA010815 to the Wistar Institute. Clinical sample acquisition was supported by NIH grant P50CA174523-02, the Wistar Institute, and the Tara Miller Foundation. O.K. was supported by an NIAID F30 fellowship (F30AI129263). This work was funded by the National Institutes of Health (AI105343, AI082630, AI115712, CA210944, AI117950 and AI108545) and the Parker Institute for Cancer Immunotherapy.

Author contributions O.K. and E.J.W. conceived the project, designed experiments and wrote the manuscript. O.K. performed the majority of the experiments described herein and performed the in vitro, in vivo and bioinformatics analysis. J.R.G. wrote the script to perform PSEA and, with S. Manne, performed pre-processing of RNA and ATAC–seq data. S. McDonald performed co-immunoprecipitation experiments for western blots. S.F.N. and K.P.P. contributed to in vivo tumour and influenza experiments. M.T.W. performed immunoprecipitation experiments for mass spectrometry. A.C.H., P.Y. and S.M.G. acquired and stained samples of human peripheral blood mononuclear cells and tumour-infiltrating $CD8^+$ T cells. J.E.W., R.P.S., J.R.G. and K.A.A. provided critical edits to the manuscript. W.X., R.K.A., X.X., G.C.K., T.C.M. and L.M.S. provided clinical samples. J.K. provided mice and intellectual input. All authors reviewed the manuscript.

Competing interests O.K. is an employee of Arsenal Biosciences. R.K.A. serves as a consultant for Sprint Biosciences, Immunacell and Array Pharmaceuticals and is a founder of Pinpoint Therapeutics. T.C.M. is an advisor to and/or receives honoraria from Aduro, Array, BMS, Incyte, Merck, and Regeneron. S.L.B. receives research funding from Celgene. E.J.W. receives honoraria, consulting fees and/or research support from BMS, Celgene, Dynavax, Eli Lilly, Elstar, Merck, MedImmune, Pieris, Roche, Surface Oncology, and KyMab. E.J.W. is a founder of Arsenal Biosciences. E.J.W. has a patent licensing agreement for the PD-1 pathway.

Additional information
Supplementary information is available for this paper at https://doi.org/10.1038/s41586-019-1325-x.
Correspondence and requests for materials should be addressed to E.J.W.
Reprints and permissions information is available at http://www.nature.com/reprints.

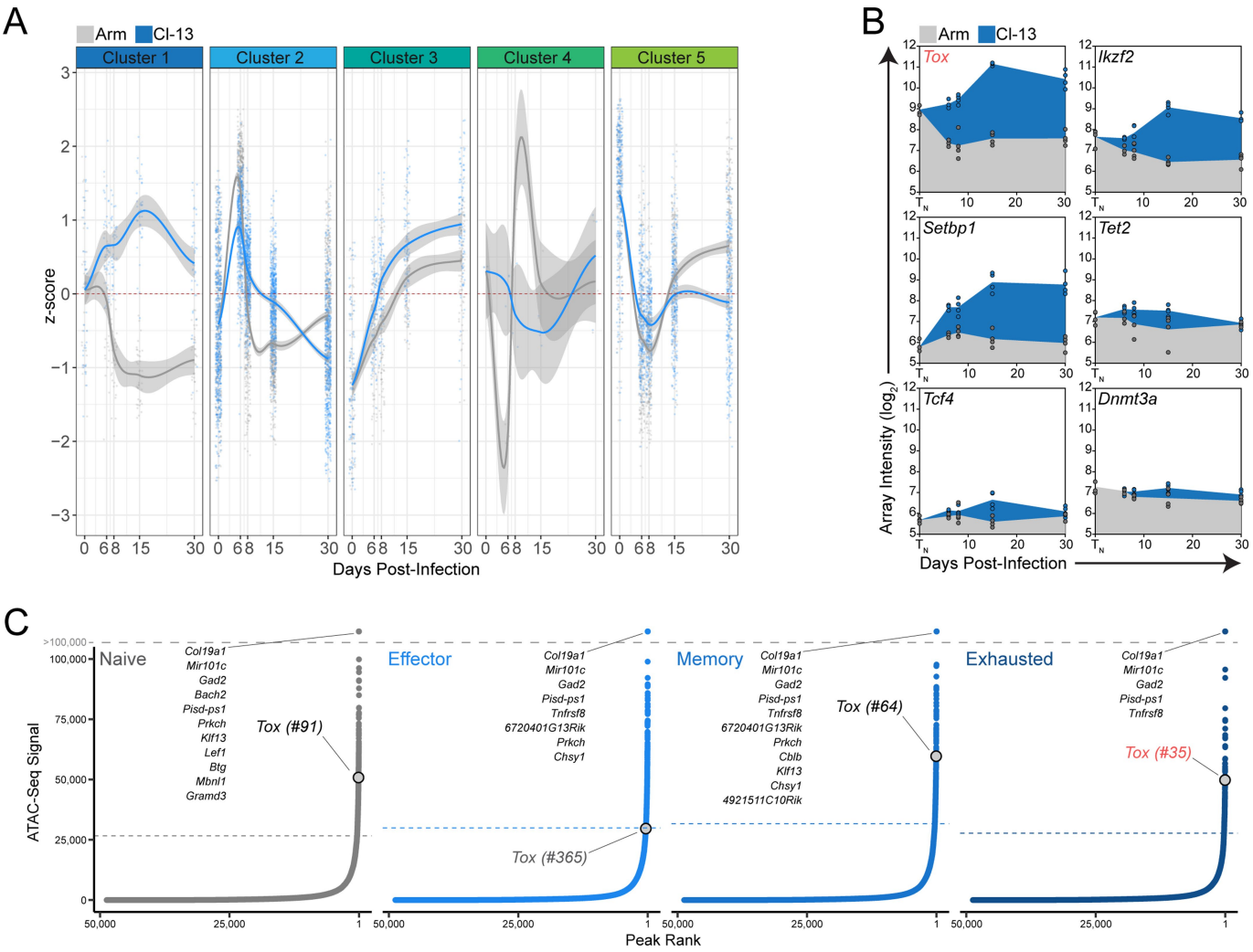

Extended Data Fig. 1 | Expression of epigenetic modifiers in acute and chronic LCMV infection. a, Data points indicate the *z*-score of each gene in clusters 1–5 plotted against time post-infection with Armstrong or clone 13. Grey and blue lines represent the moving average of *z*-score (with shading indicating the 95% confidence interval) in P14 T cells from Armstrong and clone-13 infection, respectively. **b**, Expression of selected genes within cluster 1 plotted as normalized array intensity against time post-infection. Grey and blue shading represent P14 T cells from infection with Armstrong and clone 13, respectively. **c**, Distribution of the ATAC–seq signal across loci in naive T, T_{eff}, T_{mem} and T_{ex} P14 T cells. Loci above the horizontal dashed lines denote putative super enhancers. The rank of the *Tox* locus among all identified potential super enhancers is shown.

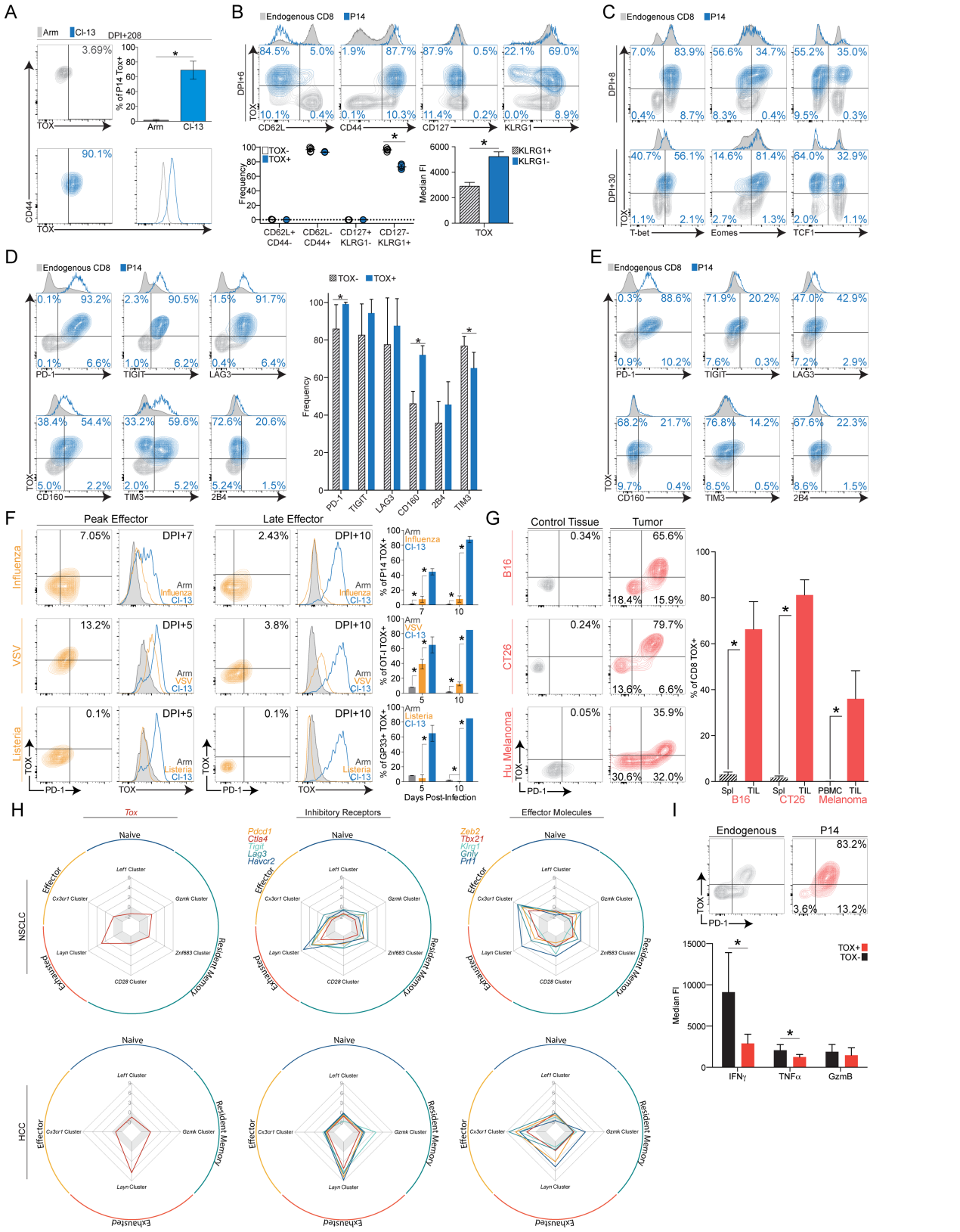

Extended Data Fig. 2 | See next page for caption.

Extended Data Fig. 2 | Dynamics of TOX expression in mouse and human disease. a, TOX expression in P14 T cells from peripheral blood at day 208 post-infection with Armstrong or clone 13. **b**, Top, T_{eff} and T_{mem} cell markers relative to TOX expression in P14 T cells or endogenous $CD8^+$ T cells on day 6 post-infection with clone 13. Bottom left, frequency of T_{mem}-cell and T_{eff}-cell subsets within TOX^+ and TOX^- P14 T cell populations. Bottom right, TOX median fluorescence intensity in $KLRG1^+$ and $KRLG1^-$ P14 T cells. **c**, TOX versus transcription-factor expression after 8 (top) or 30 (bottom) days of clone-13 infection. **d**, **e**, TOX versus inhibitory-receptor expression in P14 T cells after 8 days (**d**) or 30 days (**e**) of clone-13 infection. **f**, TOX expression in antigen-specific $CD8^+$ T cells after influenza, VSV or *Listeria monocytogenes* infection compared with LCMV Armstrong or clone-13 infection. **g**, TOX versus PD-1 and quantification of TOX expression in activated $CD8^+CD44^+$ T cells from control tissues or tumours. Control T cells for mouse tumour models were acquired from the spleen, whereas in humans, T cells from the peripheral blood of normal donors served as controls. **h**, Radar plots of median gene expression in single-cell RNA-sequencing data from tumour biopsies and peripheral blood of patients with non-small-cell lung cancer (NSCLC) or hepatocellular carcinoma (HCC)[61,62]. Median expression was calculated on cell clusters that were defined by key driver genes and represent canonical T cell populations[61,62]. **i**, Top, P14 T cell infiltration in GP33-expressing B16 tumours. Bottom, cytokine production in TOX^+ or TOX^- tumour-infiltrating P14 T cells. Contour and histogram plots are from one representative experiment of at least 2 independent experiments consisting of at least 4 mice per group. Unless otherwise noted, P14 T cells were analysed from the spleens of infected mice. In the summarized experiments, each data point represents one mouse and the error is reported as s.d. For **e**, five human melanoma biopsy samples were analysed. Statistical significance ($*P < 0.01$) was determined using the Student's *t*-test.

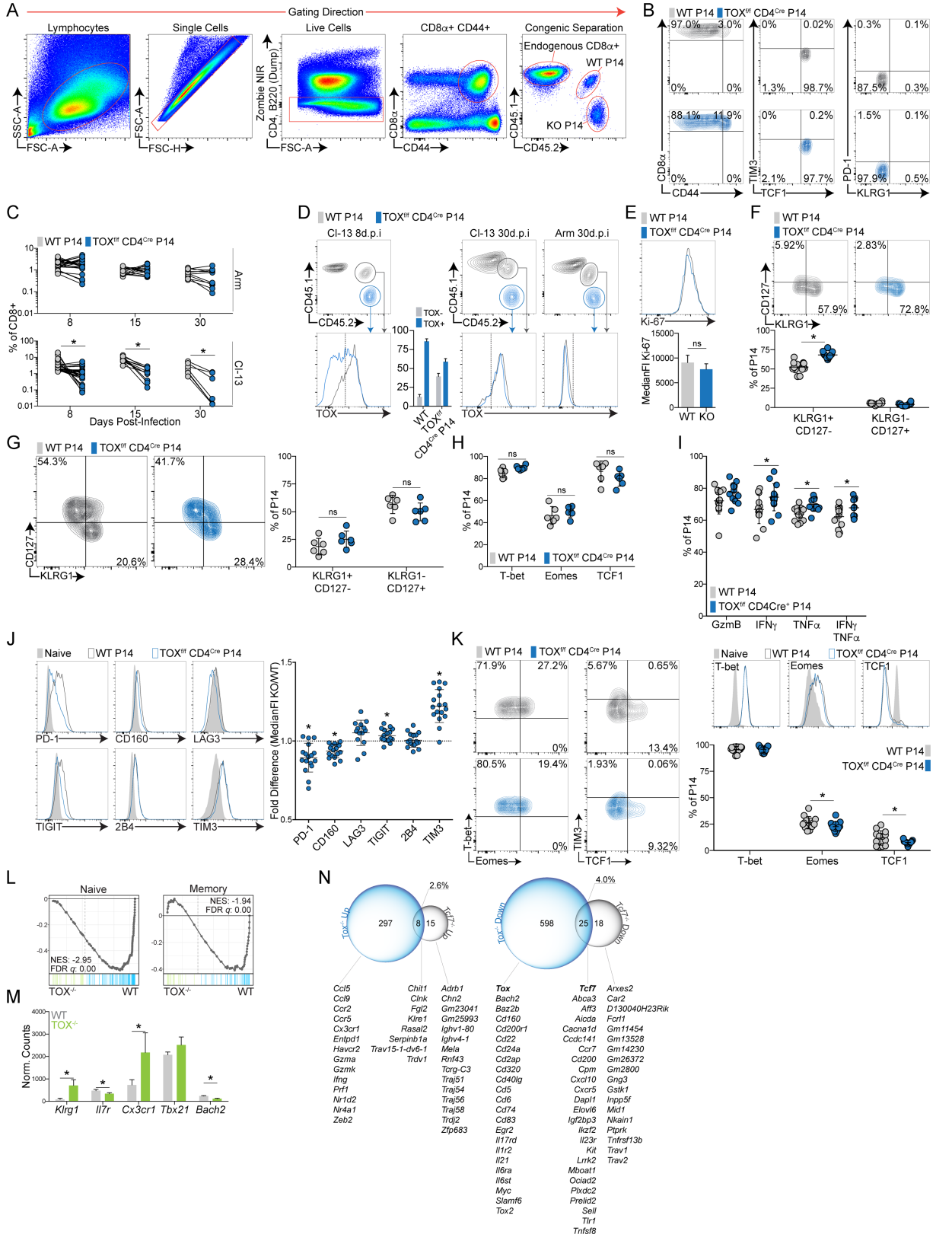

Extended Data Fig. 3 | See next page for caption.

Extended Data Fig. 3 | Response of TOX-deficient T cells in acute and chronic LCMV. a, The gating strategy used in co-adoptive transfer and infection experiments. **b**, Expression of activation markers and transcription factors in naive wild-type and $Tox^{flox/flox}Cd4^{cre}$ P14 T cells before adoptive transfer. Wild-type and TOX cKO T cells were mixed 1:1 and adoptively transferred into congenic wild-type mice followed by infection with Armstrong (**c**, **d**, **f**–**k**) or clone 13 (**c**–**e**). **c**, Frequency of wild-type or TOX cKO P14 T cells during infection with Armstrong or clone 13. **d**, TOX expression in wild-type and TOX cKO P14 T cells after infection with Armstrong or clone 13. **e**, Ki-67 expression on day 8 of clone-13 infection. **f**, **g**, Frequency of memory populations on day 8 (**f**) or day 30 (**g**) of Armstrong infection. **h**, Transcription-factor expression in wild-type and TOX cKO P14 T cells on day 30 post-infection with Armstrong. **i**–**k**, Cytokine and effector molecule (**i**), inhibitory-receptor (**j**), and transcription-factor (**k**) expression on day 8 post-infection with Armstrong. Inhibitory-receptor expression is reported as the ratio of the median fluorescent intensity between TOX cKO and wild-type P14 T cells (**j**, right). **l**, GSEA of transcriptional signatures associated with naive T or T_{mem} cells compared to the differentially expressed genes in $Tox^{-/-}$ versus wild-type P14 T cells. **m**, Expression of genes associated with the terminal short-lived subset of T_{eff} cells[26]. **n**, Comparison of the transcriptional signature of TOX cKO and TCF-1 cKO[30] T cells after 8 days of clone-13 infection. Genes differentially expressed relative to wild-type (FDR < 0.05 and log-fold change > 0.6) were compared between datasets. Contour and histogram plots are representative of at least 4 independent experiments with at least 4 mice. Statistical significance ($^*P < 0.01$) was determined by a pairwise *t*-test with Holm–Sidak correction (**c**) or the Student's *t*-test (**e**–**l**), error is reported as s.d.

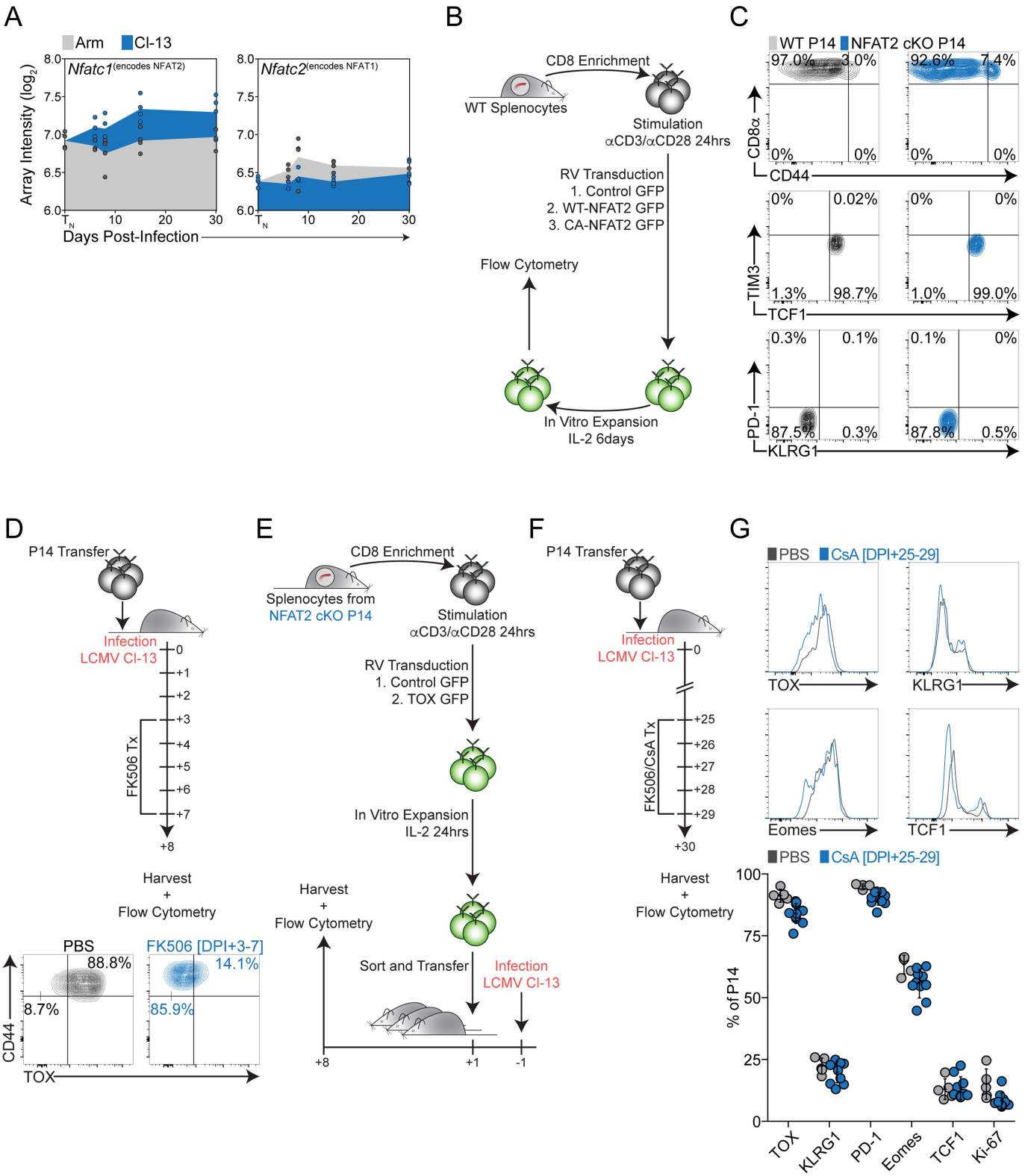

Extended Data Fig. 4 | See next page for caption.

Extended Data Fig. 4 | Effect of calcium and NFAT2 perturbation on TOX expression. a, Normalized microarray expression of *Nfatc1* (which encodes NFAT2) and *Nfatc2* (which encodes NFAT1) in P14 T cells after infection with Armstrong or clone 13. **b**, $CD8^+$ T cells were enriched, activated and transduced with control (CT), wild-type NFAT2 or CA-NFAT2 encoding retroviruses. T cells were expanded and differentiated in vitro in the presence of IL-2 for 6 days before analysis. **c**, Expression of activation markers and transcription factors in naive wild-type and $Nfatc1^{flox/flox}Cd4^{cre}$ (NFAT2 cKO) P14 T cells from the blood before adoptive transfer. **d**, P14 T cells were adoptively transferred into wild-type hosts followed by infection with clone 13. Top, on day 3–7 of infection, mice were treated with PBS or FK506 and splenocytes were collected on day 8 post-infection. Bottom, CD44 expression in P14 T cells on day 8 post-infection with clone 13 and treatment with PBS or FK506 on day 3–7. **e**, NFAT2 cKO $CD8^+$ T cells were enriched from naive mice, activated with antibodies against CD3 and CD28 and transduced with retroviruses encoding TOX or GFP-only control. Twenty-four hours later, cells were sorted and transferred into clone-13-infected mice. Protein expression was analysed on day 8 post-infection. **f**, P14 T cells were transferred into wild-type mice followed by infection with clone 13. On day 25–29 post-infection, recipient mice were treated with PBS, FK506 or cyclosporin A (CsA) and splenocytes were collected on day 30 post-infection for analysis. **g**, Protein expression in P14 T cells after treatment with cyclosporin A or PBS on day 25–29 of clone-13 infection. All contour and histogram plots are representative of at least 3 independent experiments consisting of at least 3 mice per group. Error is reported as s.d.

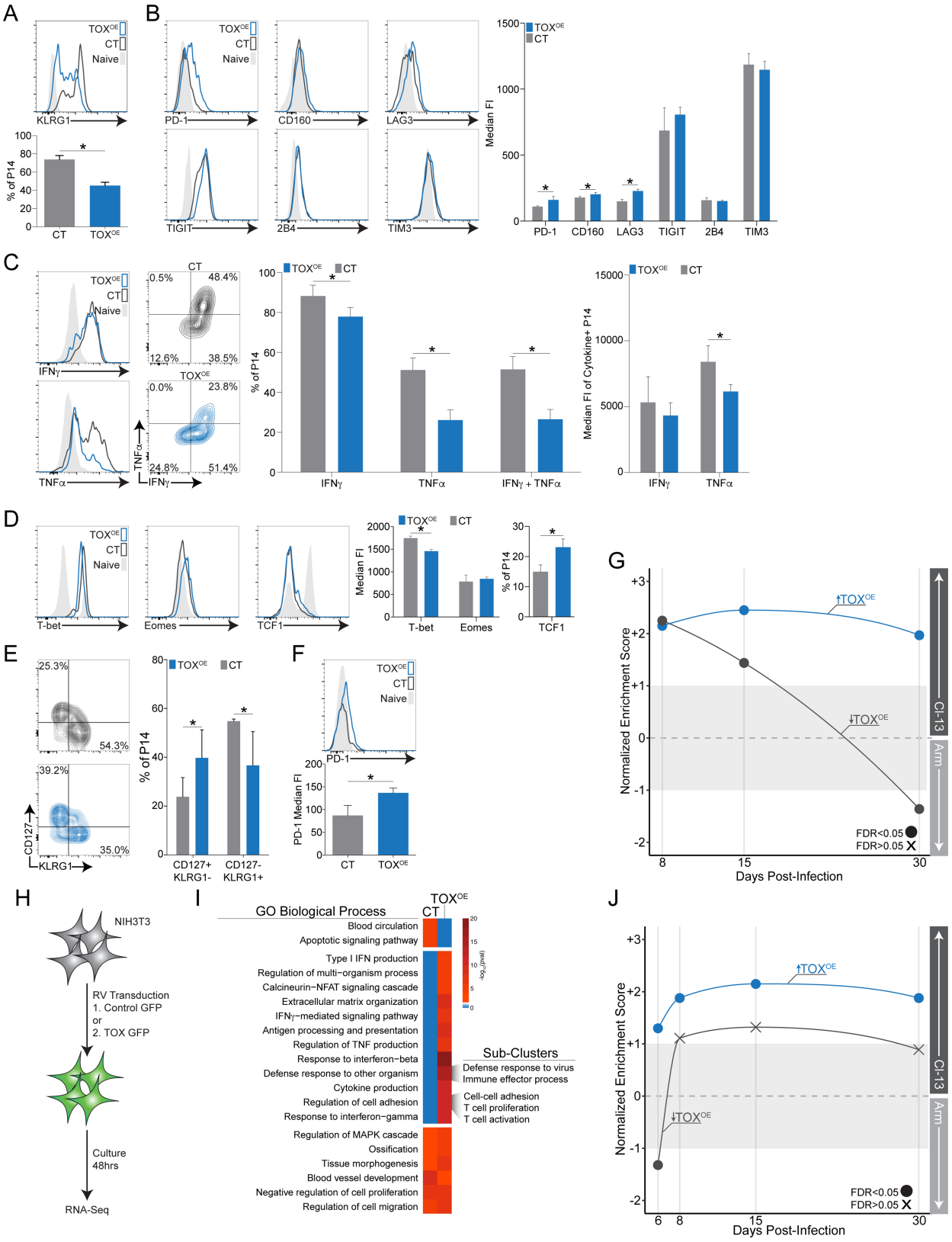

Extended Data Fig. 5 | See next page for caption.

Extended Data Fig. 5 | Enforced expression of TOX in T cells and fibroblasts. a–**d**, Naive P14 T cells were activated with antibodies against CD3 and CD28 for 24 h before transduction with retroviruses encoding TOX (TOX^{OE}) or control GFP. Twenty-four hours after transduction, GFP^{+} cells were sorted and transferred into day-2 Armstrong-infected recipients. Eight days after transfer, transduced P14 T cells were isolated from spleens and assayed for $KLRG1^{+}$ T_{eff} cell frequency (**a**), inhibitory-receptor expression (**b**), cytokine production after 5 h of restimulation with GP33 peptide (**c**) and transcription-factor expression (**d**). **e**, **f**, Distribution of memory T cell subsets and PD-1 expression in TOX- versus control-transduced P14 T cells after 30 days of Armstrong infection. **g**, Genes upregulated (blue) or downregulated (grey) in TOX^{OE} compared with control cells were analysed for enrichment in the transcripts that were differentially expressed in P14 T cells on days 8, 15 and 30 of infection with clone 13 or Armstrong[12]. Normalized GSEA enrichment scores are plotted against time post-infection. **h**, The experimental procedure used to generate the datasets analysed in **i**, **j** and Fig. 5e, f. NIH3T3 cells were transduced with retroviruses encoding TOX + GFP (TOX^{OE}) or control GFP-only. Cells were cultured for 48 h, then collected and processed for RNA-seq analysis. **i**, Gene ontology analysis of biological processes differentially regulated in TOX^{OE} versus control fibroblasts. **j**, As in **g**, genes upregulated (blue) or downregulated (grey) in fibroblasts were assayed for enrichment in the genes differentially expressed in P14 T cells on days 6, 8, 15 and 30 of infection with clone 13 or Armstrong[12]. All contour and histogram plots are representative of at least two independent experiments consisting of at least five mice per group. Unless otherwise noted, P14 T cells were analysed from the spleens of infected mice. Statistical significance ($*P < 0.01$) was determined using the Student's *t*-test, error is reported as s.d.

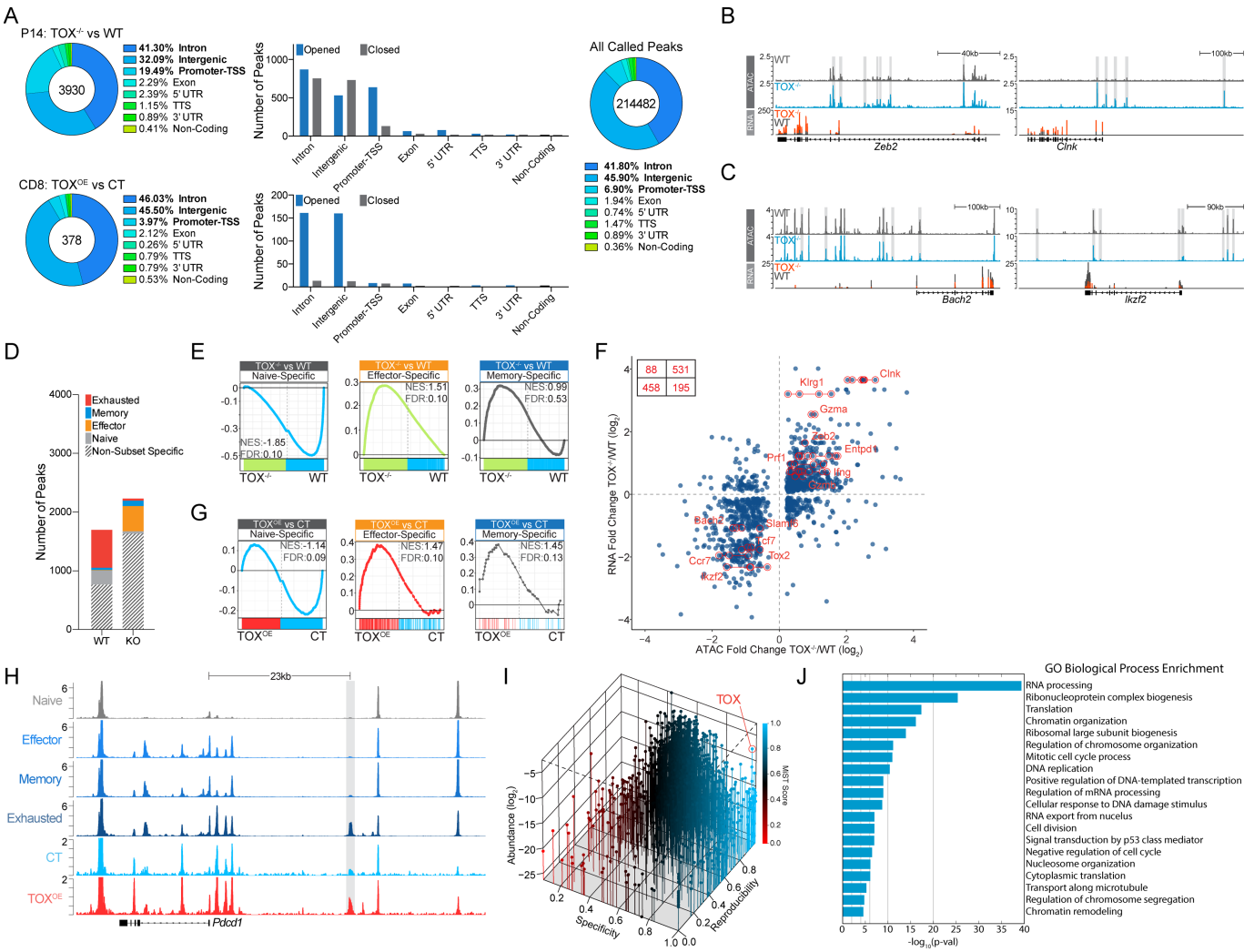

Extended Data Fig. 6 | Epigenetic program regulated by TOX. a, Left, location of differentially accessible ATAC–seq peaks from Fig. 6a (top) or Fig. 6f (bottom). Right, distribution of all peaks in CD8$^+$ T cells that are above background levels. **b**, **c**, ATAC–seq and RNA-seq tracks of T_{eff}-cell-associated (**b**) or T_{mem}-cell-associated (**c**) loci. Peaks uniquely opened (**b**) or closed (**c**) in *Tox*$^{-/-}$ relative to wild-type T cells are highlighted with grey bars. **d**, Enumeration of significantly differentially accessible sites (FDR < 0.05) in wild-type and *Tox*$^{-/-}$ T cells at T_{ex}-cell-specific and T_{eff}-cell-specific loci[13]. **e**, PSEA of chromatin regions specifically accessible in naive T, T_{eff}, T_{mem} cells[13] in *Tox*$^{-/-}$ compared with wild-type P14 T cells. **f**, Fold change in ATAC accessibility versus RNA expression. Key genes for T_{ex} and T_{eff} cells are highlighted and genes associated with multiple peaks are connected with a red line. Inset, a table enumerating the number of gene–ATAC peak pairs in each quadrant. **g**, PSEA of chromatin regions specifically accessible in naive T, T_{eff}, T_{mem} cells in TOX^{OE} compared with control P14 T cells. **h**, ATAC–seq tracks of naive T, T_{eff}, T_{mem} and T_{ex} cells[13] compared with control and TOX^{OE} T cells at the *Pdcd1* locus. The grey bar highlights the T_{ex}-cell-specific −23.8-kb enhancer. **i**, Abundance, specificity and reproducibility plot of proteins identified by mass spectrometry after TOX immunoprecipitation compared with IgG control in EL4 cells. Hits are coloured using the MiST score (blue signifies >0.75). **j**, Gene ontology biological process enrichment of TOX-bound proteins identified in **i** with MiST score >0.75.

nature research

Corresponding author(s): E. John Wherry

Reporting Summary

Nature Research wishes to improve the reproducibility of the work that we publish. This form provides structure for consistency and transparency in reporting. For further information on Nature Research policies, see Authors & Referees and the Editorial Policy Checklist.

Statistical parameters

When statistical analyses are reported, confirm that the following items are present in the relevant location (e.g. figure legend, table legend, main text, or Methods section).

n/a	Confirmed	
☐	☒	The exact sample size (*n*) for each experimental group/condition, given as a discrete number and unit of measurement
☐	☒	An indication of whether measurements were taken from distinct samples or whether the same sample was measured repeatedly
☐	☒	The statistical test(s) used AND whether they are one- or two-sided *Only common tests should be described solely by name; describe more complex techniques in the Methods section.*
☐	☒	A description of all covariates tested
☐	☒	A description of any assumptions or corrections, such as tests of normality and adjustment for multiple comparisons
☐	☒	A full description of the statistics including central tendency (e.g. means) or other basic estimates (e.g. regression coefficient) AND variation (e.g. standard deviation) or associated estimates of uncertainty (e.g. confidence intervals)
☐	☒	For null hypothesis testing, the test statistic (e.g. *F*, *t*, *r*) with confidence intervals, effect sizes, degrees of freedom and *P* value noted *Give P values as exact values whenever suitable.*
☐	☒	For Bayesian analysis, information on the choice of priors and Markov chain Monte Carlo settings
☐	☒	For hierarchical and complex designs, identification of the appropriate level for tests and full reporting of outcomes
☐	☒	Estimates of effect sizes (e.g. Cohen's *d*, Pearson's *r*), indicating how they were calculated
☐	☒	Clearly defined error bars *State explicitly what error bars represent (e.g. SD, SE, CI)*

Our web collection on statistics for biologists may be useful.

Software and code

Policy information about availability of computer code

Data collection	Flow cytometry data were collected on LSR II or FACSAria instruments with FACSDiva software v8.0.1 (BD)
Data analysis	Flow cytometry data were analyzed on FlowJo v10.4.2 (TreeStar) and statistical analysis performed on Prism v6.0 (GraphPad). Genomic analyses were performed using R Studio v3.4.3 and all packages utilized were updated to most current versions. Custom script locations have been noted in the methods section.

For manuscripts utilizing custom algorithms or software that are central to the research but not yet described in published literature, software must be made available to editors/reviewers upon request. We strongly encourage code deposition in a community repository (e.g. GitHub). See the Nature Research guidelines for submitting code & software for further information.

Data

Policy information about availability of data

All manuscripts must include a data availability statement. This statement should provide the following information, where applicable:

- Accession codes, unique identifiers, or web links for publicly available datasets
- A list of figures that have associated raw data
- A description of any restrictions on data availability

Data availability statement is located in methods section.

Field-specific reporting

Please select the best fit for your research. If you are not sure, read the appropriate sections before making your selection.

☒ Life sciences ☐ Behavioural & social sciences ☐ Ecological, evolutionary & environmental sciences

For a reference copy of the document with all sections, see nature.com/authors/policies/ReportingSummary-flat.pdf

Life sciences study design

All studies must disclose on these points even when the disclosure is negative.

Sample size	Sample sizes were based on those used in previous and preliminary studies from our lab. For all animal experiments, we expected to see at least a ~50% difference relative to control populations. Therefore, sample sizes of n=3-7 were chosen to allow for the determination of this difference (t-test, α set at 0.05). Additional 1-3 mice were used per experimental group for LCMV and LM infection experiments to compensate for mortality.
Data exclusions	No data were excluded from analyses
Replication	All experiments presented in this study were performed using at least 2 biological replicates. All presented results were repeatable.
Randomization	Adoptive transfer and infection experiments were randomized by selecting recipient mice at random from a pool of >8 for each experiment.
Blinding	Blinding was not relevant to these studies

Reporting for specific materials, systems and methods

Materials & experimental systems

n/a	Involved in the study
☒	☐ Unique biological materials
☐	☒ Antibodies
☐	☒ Eukaryotic cell lines
☒	☐ Palaeontology
☐	☒ Animals and other organisms
☐	☒ Human research participants

Methods

n/a	Involved in the study
☒	☐ ChIP-seq
☐	☒ Flow cytometry
☒	☐ MRI-based neuroimaging

Antibodies

Antibodies used	Antibodies used in this work are listed in the methods section
Validation	Antibodies were validated by the manufacturer. TOX antibodies were validated by performing mass spectrometry on bands positively stained in EL4 lysates.

Eukaryotic cell lines

Policy information about cell lines

Cell line source(s)	ATCC
Authentication	*Describe the authentication procedures for each cell line used OR declare that none of the cell lines used were authenticated.*
Mycoplasma contamination	All cell lines were tested for mycoplasma contamination prior to use in experiments
Commonly misidentified lines (See ICLAC register)	NA

Animals and other organisms

Policy information about studies involving animals; ARRIVE guidelines recommended for reporting animal research

Laboratory animals	Laboratory animals used in this study are described in the methods section
Wild animals	Study did not involve wild animals
Field-collected samples	Study did not involve samples collected in the field

Human research participants

Policy information about studies involving human research participants

Population characteristics	Please refer to methods for this information.
Recruitment	Please refer to methods for this information.

Flow Cytometry

Plots

Confirm that:

☐ The axis labels state the marker and fluorochrome used (e.g. CD4-FITC).

☒ The axis scales are clearly visible. Include numbers along axes only for bottom left plot of group (a 'group' is an analysis of identical markers).

☒ All plots are contour plots with outliers or pseudocolor plots.

☒ A numerical value for number of cells or percentage (with statistics) is provided.

Methodology

Sample preparation	This information is provided in the methods section.
Instrument	This information is provided in the methods section.
Software	This information is provided in the methods section.
Cell population abundance	This information is provided in the methods section.
Gating strategy	Refer to Extended Data Figure 3a for gating strategy.

☒ Tick this box to confirm that a figure exemplifying the gating strategy is provided in the Supplementary Information.